Chapter II

N-acetyl-d-glucosamine (NADG) decorated nano-lipid-based carriers (NLBCs) as theranostics module for targeted anti-cancer drug delivery

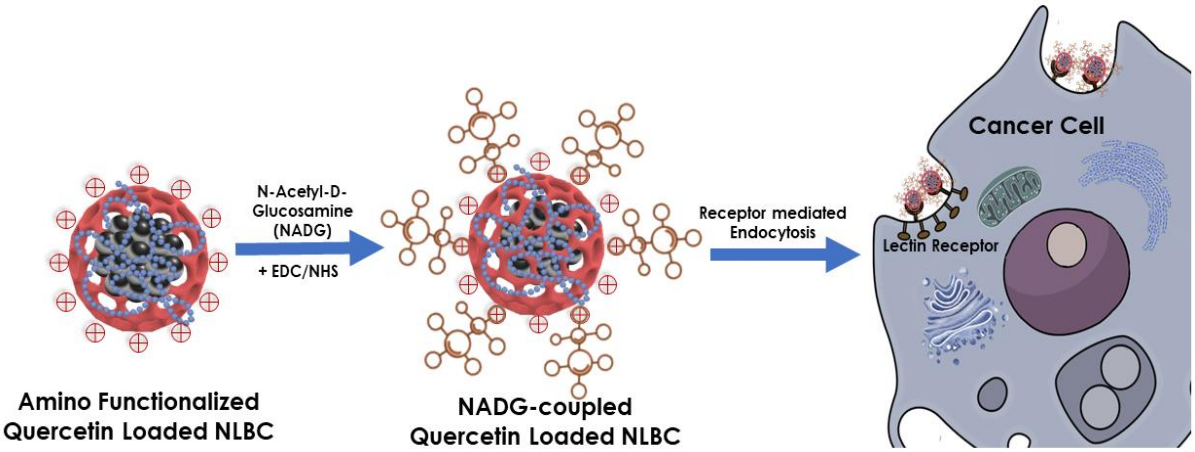

Rahul Kumar et al., ***Materials Chemistry and Physics.*** *282 (2022) 125956. doi.org/10.1016/j.matchemphys.2022.125956.*

Candidate CRediT and collaborators contribution statement

Rahul Kumar: Data curation, formal analysis, investigation, methodology, writing – thesis, review & editing, and conceptualization.

Collaborators: Review & editing, resource, validation, and software.

1. Introduction

Poor solubility, bioavailability, physiological, physicochemical, and pharmaceutical barriers are major problems allied with free drugs. Besides these limitations, multiple drug resistance is a major challenge associated with them. All these limitations could be overcome through the novel material-based system comprising a ligand-based liposomal formulation of drugs, which has shown great promise in recent years **[1]**. Ligand-based drug delivery construct has the potential to accumulate more drugs inside the targeted cells through receptor-mediated endocytosis **[2]**. Cancer cells overexpressed the lectin-like receptor having greater affinity to the carbohydrate moieties **[3]**. To date, different carbohydrate moieties have been used as a ligand to target the receptor expressed on the cancer cells. During glycosylation, cancer cells over-expressed the receptor for various carbohydrate molecules greatly, for instance, fucose, galactose, mannose, etc. **[3,4,5]**. The glycans when coupled with several drug-loaded nanocarriers result in the formation of glycosylated transporter. This comprises an anchored ligand that helps in the faster intake of drugs inside the cancer cells through receptor-mediated endocytosis **[6,7]**. Consequently, developing a monosaccharide N-Acetyl-D-glucosamine (NADG)-anchored material system could be a potential approach for the effective transport of drugs to the cancer cells. Numerous malignant cells, including MCF-7, overexpressed the lectin receptor greatly compared to the normal cells on their surfaces, which has been well documented **[8]**. The NADG has a high affinity for lectin molecules and specifically binds to these molecules **[9]**. Hence, the MCF-7 cells can be used as a model system to demonstrate the lectin receptor-mediated endocytosis.

In view of this, the delivery of anti-cancer drugs upon loading in the diverse delivery vehicle has been investigated. In general, micelles **[10]**, microspheres **[11]** liposomes, **[12]**, nanoparticles **[13]**, and dendrimers **[14]** have been employed as drug delivery vehicles. Nano lipid-based carriers (NLBCs) have emerged as the most facile and efficient vehicle to overcome

the physicochemical and physiological barriers. Moreover, this type of material could also shield the drug from elimination in the circulatory system and have acceptable regulatory and safety profiles. Also, NLBCs have unique characteristics such as biocompatibility, biodegradability, controlled drug release, and the small particle size ranges from 50 nm to 1000 nm **[15]**. Hence, these criteria qualify NLBCs to be a potent drug carrier for cancer theranostics as a whole.

Several kinds of research regarding polyaminoacid-coated liposomes delivery have been reported that has been administered intravenously **[16,17]**. The main reason for using poly-amino acid coating on the surface of liposomal vesicles is to facilitate the prolonged circulation in the blood and provide the platform through which the ligand is coupled. Moreover, it also helps in the precise release of drugs from liposomes and stabilizes the liposomal structure **[18]**. Hence, in the present study, poly-L-lysine are coated with NLBCs through a charge interaction method.

Free radicals are important molecules present during cell damage, which can be generated either through normal cell metabolism or external sources (pollutants, smoke, heavy metals, herbicide, pesticides, etc.). In living cells, certain enzymes, e.g., xanthine oxidase, amino acid oxidase are responsible for generating the free radicals. However, oxygen molecules can also react with certain organic molecules non-enzymatically during oxidative phosphorylation and generate free radicals **[19]**. The scavenging activity of antioxidants can inhibit free radicals produced from the oxidation reaction of molecules. Antioxidants are one of the most frequently used anti-cancer agents and have been used for such purposes in recent years **[20]**. In view of drug transport for cancer remedies, Quercetin (Q) has the major potential for antioxidant activity **[21]**. In the present investigation, we constructed a nano biomaterials-based carrier for drug delivery. The Q is loaded inside the core and the subsequent layer of NLBCs. Poly-L-lysine is anchored on the surface of NLBCs through charge interaction, and

the NADG is coupled to poly-L-lysine through classical bioconjugation chemistry-based cross-linking **[22]**. Moreover, the *in vitro* cell viability of NADG-Q-NLBCs was critically examined, and the effects were compared with the free Q and NLBCs. In a previous study, the effectiveness of biopolymer-mediated drug delivery on MCF-7 cells was reported **[23]**. **Fig. 2.1** shows the schematic representation of the N-acetyl-D-glucosylated Q-loaded NLBCs fabrication process and its interaction with the cancer cell.

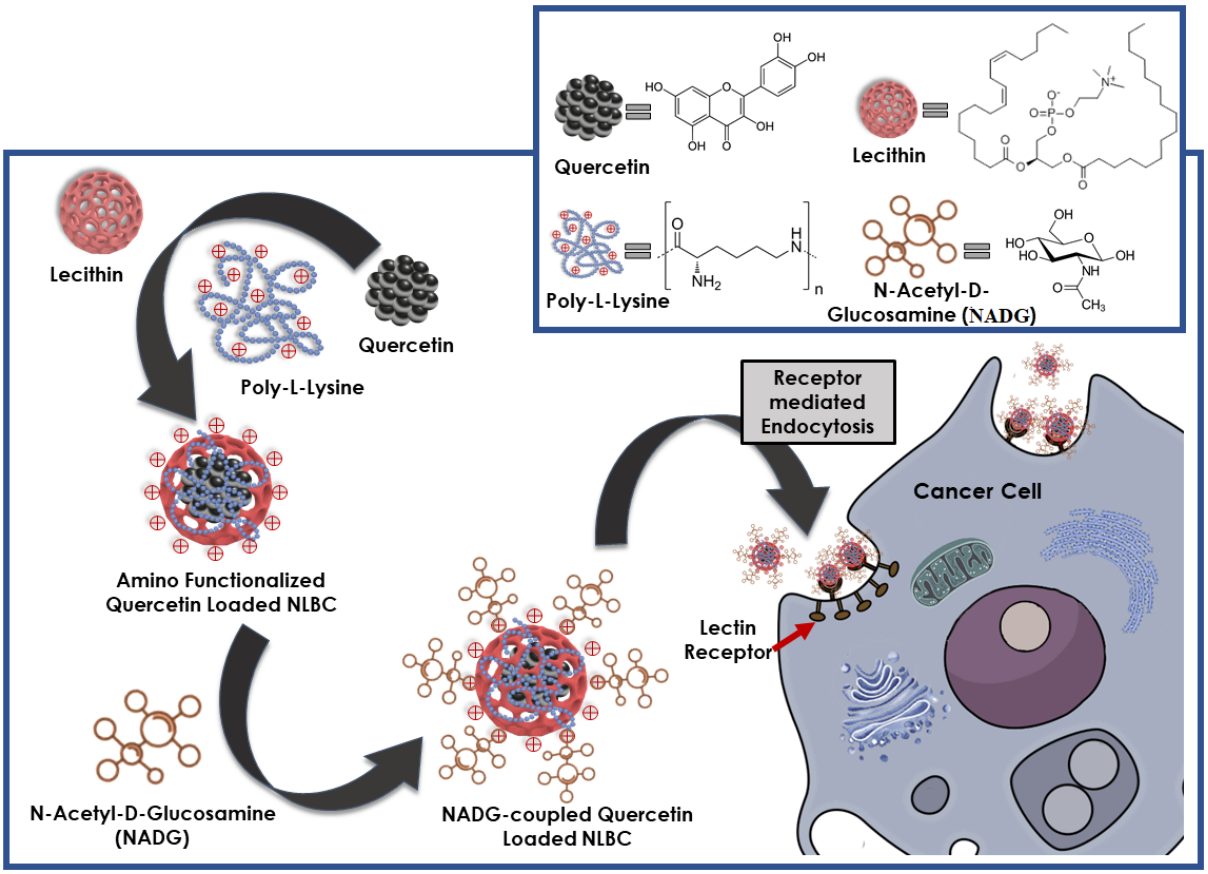

Figure 2.1. Schematic representation of the synthesis of N-acetyl D-glucosylated Q-loaded nano lipid-based carrier and its cellular internalization through receptor-mediated endocytosis.

2. Materials and methods

2.1. Materials

Soya lecithin (PC), Poly-L-lysine, and N-acetyl-D-glucosamine were obtained from Merck., EDTA/trypsin, Quercetin, 3-(4,5-dimethylthiazol-2-yl)-2,5-diphenyltetrazolium bromide (MTT), fetal bovine serum (FBS), and chloroform were obtained from Sigma-Aldrich.

Phosphate buffer, streptomycin, penicillin, and dimethyl sulfoxide were purchased from HiMedia. EDC.HCL 1-ethyl-3-(3-dimethylaminopropyl) carbodiimide hydrochloride and NHS (N-hydroxysuccinimide) were obtained from Thermo Fisher Scientific. Breast cancer cells (MCF-7) were obtained from NCCS (National Centre for Cell Sciences), Pune, India. The rest of the solvents and reagents were either analytical or HPLC grade and were used without any purification step.

2.2. Fabrication of Q laden NLBCs

A single emulsion solvent evaporation method with modification was used to fabricate NLBCs. Briefly, soya lecithin (200mg) and Q (5.0 mg) were dissolved in 10.0 mL of chloroform at 65.4° C. The resulting suspension was kept over a magnetic stirrer at 1000 rpm for 10 min. Subsequently, poly-L-lysine (12.0 mol%) was mixed into the solution and stirred for another 10 min at 1000 rpm to obtain the pure organic phase. The organic phase, containing lipid and poly-L-lysine, was then added dropwise from a particular height (20.0 cm) through a syringe into a preheated aqueous solution (5.0 % dextrose, 0.8% saline, and distilled water) under magnetic stir at 1,000 rpm for 3 h. Further, the solution was allowed to sonicate using a probe sonicator (model no. ATP-120, Hielscher Ultrasonics GmbH, Teltow, Germany) for 3 min under the ice surrounding vessel. The fabricated lipid carriers were separated using centrifugation at 7,828g for 20 min at 4.0° C. The obtained debris was carefully cleaned three times with distilled water to remove unbound poly-L-lysine and free drugs. The obtained suspension was kept at -80.0° C overnight, and the frozen dispersion was lyophilized (Labcanco, catalog NO. 7740060, LABCONCO Corporation, Kansas City, MO, USA) for further use.

2.3. Preparation of N-acetyl-D-glucosylated Q-loaded NLBCs

NADG was anchored to the surface of NLBCs modified with poly-L-lysine through EDC/NHS cross-linking. In this method, first, the ring structure of NADG was opened and further cross-linked with poly-L-lysine through the EDC/NHS bioconjugate chemistry **[24,25,26,27,28]** which results in the formation of an amide bond. In the first step, NADG (8.0 µM) was added in 0.2 M sodium acetate buffer (pH 4.0) at 65.0°C. Next, the poly-L-lysine coated NLBCs formulation was added, followed by the addition of EDC/NHS (2:1) to the mixed suspension, and the formulation was kept on the magnetic stirrer for 8 h at 1000 rpm. This leads to the conjugation of NADG to the NLBCs modified with poly-L-lysine, and the resulting solution was subjected for centrifugation at 7,828g for 15 min under 4.0°C. The obtained precipitate was cleaned with distilled water twice to remove the unbound NADG. The resulting nano-bioconjugate was stored overnight at -80.0°C followed by freeze-drying through a lyophilizer. **Fig. 2.2** shows the chemical reaction for NADG conjugation with poly-L-Lysine.

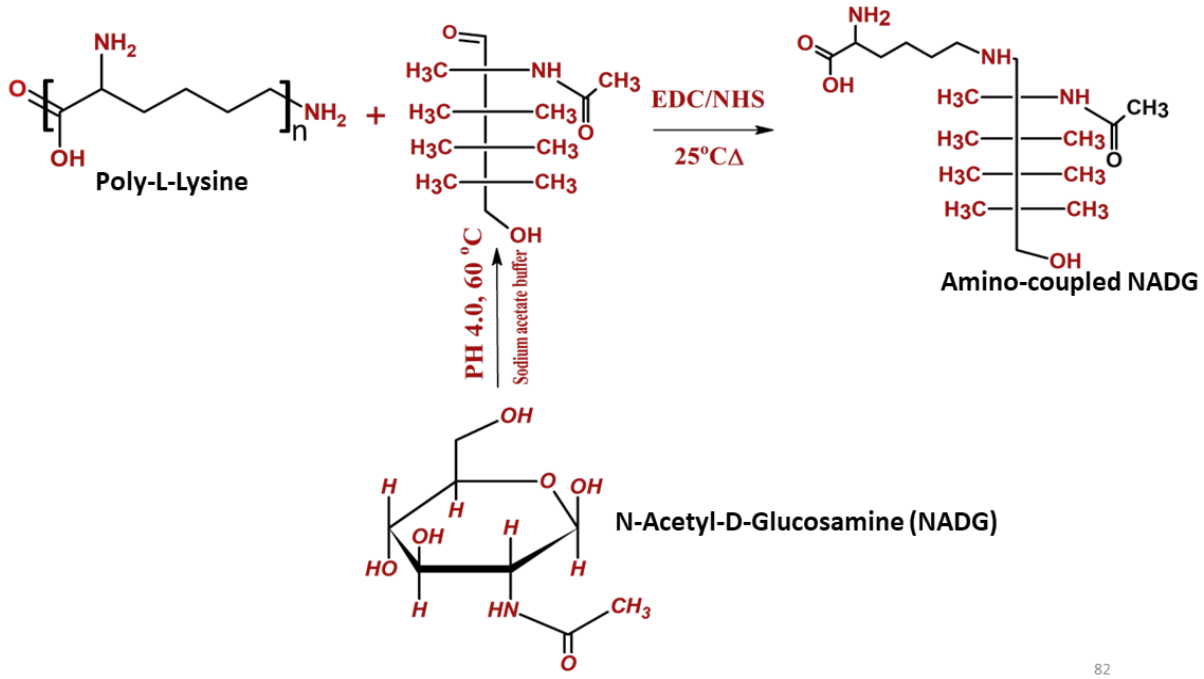

Figure 2.2. Chemical reactions for N-acetyl D-glucosamine with Poly-l lysine

2.4. In vitro fluorescence study using lectin-NADG nano-bioconjugate

The fluorescence analysis of lectin in the absence and presence of NADG was investigated using the FP-8300 fluorescence spectrophotometer (Spectroscopy Scientific NZ Ltd., Christchurch, New Zealand). The spectrophotometer was equipped with a Xe arc lamp (150 W), and monochromatic light passed through quartz (fluorescence-free) of path length 1.0 cm at the physiological temperature. Before recording the fluorescence spectra, the lectin-NADG solution was incubated for 10 min for all the titration experiments. The fluorometric titrations of lectin (1.0×10^{-6} M) were started with NADG (1.0×10^{-5} M). The fluorescence spectra were recorded with the incremental addition of NADG between 5.0×10^{-8} M and 4.0×10^{-7} M. The lectin molecules were stimulated at 280 nm at room temperature. The emission spectra were collected between 290 nm and 410 nm (pH 7.2). We have also evaluated the interaction between lectin-NADG quantitatively to verify the stability of the developed lectin-NADG nano-bioconjugate using these fluorescence signals. We have numerically evaluated the binding between lectin molecules and NADG using equation (1).

$$\log (F_0\text{-}F)/F = \log K + n \log [\text{NADG}] \qquad \ldots\ldots\ldots Eq.\ 1$$

In the equation, F_0 is denoted for the fluorescence intensity of free lectin molecules, whereas F indicates fluorescence intensity on the progressive addition of NADG. K denotes the binding constant, and n represents the binding site

2.5. Encapsulation efficiency and percentage of drug loading

The encapsulation efficacy of Q in Q-NLBCs and NADG-Q-NLBCs was determined by the amount of unattached Q present in the solution using the dialysis technique **[21]**. The standard formulation and developed nano-bioconjugates were transferred into a dialysis tube (MWCO 10000 Da) in separate experimental settings. They were kept on a magnetic stirrer to allow the dialysis at 60 rpm for 1 h against double distilled water. Sink condition was maintained

throughout the dialysis to remove the unencapsulated drugs from the carrier. The sample was then centrifuged for 20 min at 17,615g to separate the pellet and the supernatant. The pellet was collected and cleaned thoroughly with distilled water three times. The washed debris was kept overnight at -80.0°C and subsequently freeze-drying using a lyophilizer. Lyophilized powder of Q-NLBCs and NADG-Q-NLBCs was dissolved in chloroform separately vortexed for 2 min after centrifugation at 1,957g for 15 min. A membrane (0.45 µm) was used to filter the supernatant, and the filtered supernatant was poured into HPLC vials (Merck), loaded into the HPLC system (HITACHI D-6500, Hitachi Ltd., Chiyoda-ku, Tokyo, Japan) for quantification of Q entrapped within the Q-NLBCs and NADG-Q-NLBCs. Drug encapsulation efficiency (EE%) and percentage of drug loading (DL%) in both systems were numerically calculated using equation (2) and equation (3), respectively.

$$\mathrm{EE}(\%) = \frac{\text{Amount of Q added} - \text{Amount of Q in the collected sample}}{\text{Amount of Q added}} \times 100 \qquad \text{…….. } \textit{Eq. 2}$$

$$\mathrm{DL}(\%) = \frac{\text{Mass of Q}}{\text{Mass of particles}} \times 100 \qquad \text{…….. } \textit{Eq. 3}$$

2.6. Scanning Electron Microscopy (SEM) Imaging of nano-bioconjugate

The surface morphology of Q-NLBCs and NADG-Q-NLBCs was studied using SEM (Evo-Scanning Electron Microscope MA15/18, Carl Zeiss Microscopy LTD, Jena, Germany). The SEM was operated with an accelerating voltage of 26.00 kV. In brief, 10.0 µl suspension of Q-NLBCs and NADG-Q-NLBCs was taken on the rectangular slide and allowed to dry

separately. The samples were then gold-coated to allow conductivity. Subsequently, the conductive sample was kept on a copper stub before obtaining the images.

2.7. Analysis of particle diameter and charge distribution

Dynamic Light Scattering (Zeta Nano S Red badge, Malvern Panalytical Ltd. Worcestershire, United Kingdom) was used to determine the diameter and the charge of Q-NLBCs and NADG-Q-NLBCs in an aqueous solution. In brief, suspension of Q-NLBCs, and NADG-Q-NLBCs were individually diluted twelve times with solvent. The diluted suspension was then placed under a probe sonicator and allowed to sonicate for 2 min at 40.0 % amplitude under the ice surrounding vessel. Sonicated sample was placed in polystyrene cuvettes, and the size of the particle (nm) was analyzed at a fixed angle of 90° at room temperature.

2.8. Infrared spectroscopy (IR) characterization of nano-bioconjugate

An infrared spectrum of Q-NLBCs and NADG-Q-NLBCs was examined with IR (Nicolet iS5, Thermo Electron Scientific Instruments LLC, Madison, USA) to confirm the numerous functionalities (OH, CH_2, PO_4^{3-}, NH_2, NH-CH_2) intact with them. Briefly, 13.0 mm pellets were prepared using a hydraulic press (HP-15-TM; HP-mini), generating 15.0 tons of force. While preparing the pellets, the dried samples of Q-NLBCs and NADG-Q-NLBCs were loaded separately with the IR grade KBr (potassium bromide). Subsequently, the prepared pellets were scanned starting from wavenumber 4000 cm^{-1} to 400 cm^{-1}, and data were recorded.

2.9. X-ray diffractometry (XRD) characterization of nano-bioconjugate

XRD (Rigaku SmartLab 9kW Powder type, RIGAKU Corporation, Tokyo, Japan) was conducted to study the crystal or polycrystalline structure of NLBCs, and NADG-Q-NLBCs. A Cu Kα radiation source, operating at 30kV/15mA was used. Diffractogram was obtained by X-ray scanning starting from initial angle $2\theta = 2°$ to $2\theta = 90°$ at a scanning speed of $2° \text{ min}^{-1}$. All the parameters during the experiment were fixed at room temperature.

2.10. In vitro drug release study of nano-bioconjugate

The *in vitro* drug release investigation was undertaken to assess the percentage of drug release following lipid degradation. This is one of the most important *in vitro* experiments that may provide the information of drug release patterns that can be a basis for treating the nano-bioconjugate in the cellular system. Briefly, 5.0 mg of NADG-Q-NLBCs formulation was dissolved in 2.5 mL of PBS at the physiological pH. Subsequently, the suspension was poured inside the dialysis tube with a molecular cut-off of 10,000 Da. Dialysis was performed using a sterilized beaker in 150.0 mL of PBS where the dialysis tube was placed horizontally, and the system was maintained at 37.0°C at 100 rpm for 200 h. A portion of the sample was collected and replaced with the same portion of the PBS at regular intervals. The collected sample was stored separately. The UV-spectrophotometer was used to quantitatively estimate the amount of drug release using the standard calibration plot of the drug obtained at 510 nm (figure not shown).

2.11. Cell culture and assessment of in vitro cell toxicity

MCF-7 cells were cultivated in DMEM (Dulbecco's Modified Eagle Medium) accompanied with 10.0 % fetal bovine serum (FBS), 2.0 mM glutamine, 100 U/mL penicillin, 100 U/mL streptomycin, 1.0 mM sodium pyruvate, and 50.0 µM 2-mercaptoethanol. Cells were maintained in a Forma^{TM} steri-cycle^{TM} CO_2 incubator (P 190, LEEC Ltd., Nottingham, UK) with the atmospheric condition of CO_2 (5.0 %) at 37.0 ^{0}C. Next, the cell toxicity of the developed nano-bioconjugates was evaluated using the MCF-7 cells by the MTT assay. In a multi-well plate, cells were cultivated at a density of 4×10^5 cells/well and cultured for 24 h. The cells were further seeded in the 12-well plate with the fresh media. To validate the results, treatments were given in five separate experiments where each group contained NLBCs, free Q, and NADG-Q-NLBCs. The Q concentration in the first, second, third, fourth, and fifth set

of experiments was 2.0, 4.0, 6.0, 8.0, and 10.0 µg/mL, respectively. To confirm the role of nano-bioconjugate, the same Q concentrations were loaded while preparing the NADG-Q-NLBCs. The treated cells were incubated in the CO_2 incubator at a 5.0 % CO_2 concentration for 48 h for all the experiments. Subsequently, cells were washed twice with distilled water to separate the residual amount of the NLBCs, free Q, NADG-Q-NLBCs in the respective experiments. Cells were further treated with freshly prepared 12.0 µl of MTT in PBS (5.0 mg/mL) and kept in the incubator for 4 h at 37.0°C. After that, cells were dissolved in DMSO to dissolve the formazan crystals, and the calorimetric analysis was performed to estimate the viable cells at 595 nm.

2.12. Testing of statistical significance

Analysis of variance was made to assess the findings of the experiment. One-way analysis of variance compares the mean of two or more than two groups and check the null hypothesis. The experiment was performed in replicate. Values are reported as (mean ± standard error) and significance level as ($^{***}p< 0.001$, $^{**}p<0.01$ and $^{*}p<0.05$).

2.13. Flow cytometry analysis

Annexin V conjugated with FITC and PI solution were used to distinguish the early and late apoptosis cells induced by NLBCs, Q-NLBCs, and NADG-Q-NLBCs. Briefly, cells were cultured at a cell density of 1×10^5 cells/mL after being harvested. Further, cells were grown in a multi-well plate with a fresh medium containing NLBCs, Q-NLBCs, and NADG-Q-NLBCs at 10.0 µg/mL Q concentration. The multi-well plate was kept in the incubator for 48 h; then, the cells were washed twice to remove the residual amount of NLBCs, Q-NLBCs, NADG-Q-NLBCs. After washing, the cells were allowed for cold trypsinization and were harvested using centrifugation. These cells were washed twice to remove the trypsin and resuspended in binding buffer (1X). Consequently, the annexin V conjugated with FITC and propidium iodide

solutions were sequentially added to the cells following the incubation for 30 min at 25.0°C in the dark. The percentage of viable, apoptotic (early and late), and necrotic cells was calculated using a flow cytometer (BD LSR Fortessa TM San Jose, BD biosciences, CA, USA). The annexin-V-PI staining was analyzed using the FL-2 or FL3 channel, acquiring 20,000 events for each sample.

3. Results and Discussion

3.1. Fluorescence studies

Fluorescence studies were performed initially to validate the interaction between the lectin molecules and NADG. For this purpose, standard solutions were prepared, and interaction was studied in a dose-dependent manner (**Fig. 2.3a**). In fluorimeter, the fluorescence emission from aromatic amino acids intact in the core of lectin molecules is recorded when excited at a particular wavelength. The reduction of the fluorescence intensity of aromatic amino acids interprets their conformational changes. The quenching of the fluorescence intensity results from NADG binding with lectin molecules. The lectin molecules emit a fluorescence signal at λ_{max} = 325 nm once excited at λ = 280 nm (red curve). The emission strength of lectin molecules was reduced progressively when NADG was added gradually at an increasing concentration (blue curves).

A graph was plotted between log (F_0– F)/F along Y-axis and log [NADG] along X-axis (**Fig. 2.3b**) which shows the correlative relationship and represents the regression equation as follows: log (F_0-F)/F= 6.823 ± (0.349) + 1.107 ± (0.052) [log (NADG)] with the correlation coefficient (R^2) of 0.98. The slope and intercept values reflect the binding site and binding constant. The binding constants *K* and binding site *n* (lectin-NADG complexes) at physiological pH were recorded to be 6.823 ± 0.349 M^{-1} and 1.107 ± (0.052), respectively. The

above results confirmed that lectin has an affinity for NADG in experimental settings. The NADG has been further utilized for the theranostics application in the present study.

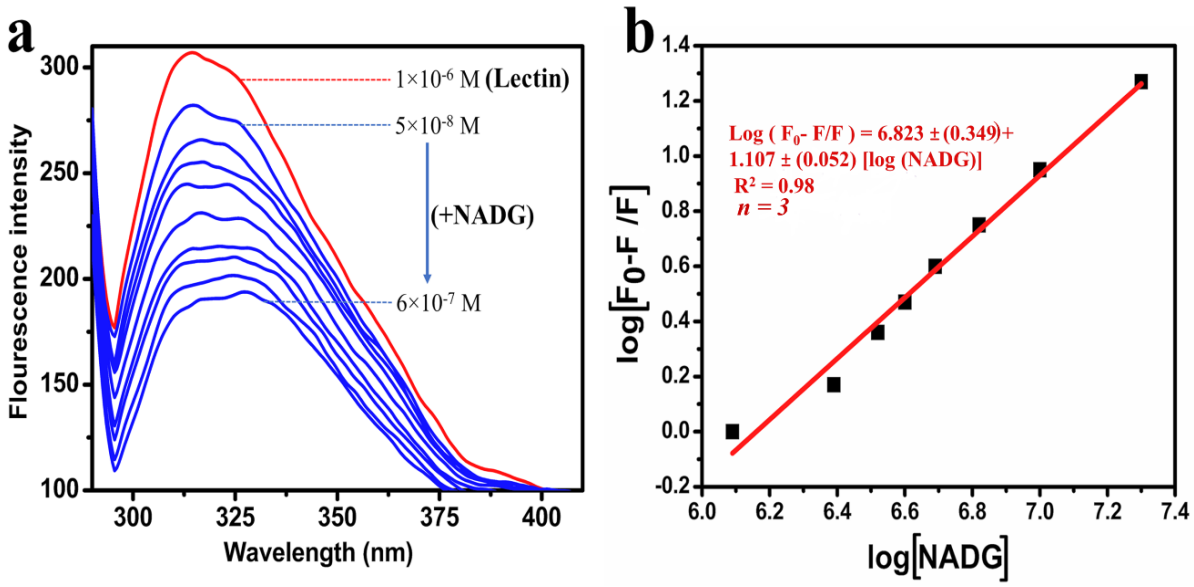

Figure 2.3. Fluorescence spectroscopy emission spectra of the lectin-NADG complex. (a) Emission spectra of lectin reduced on gradual addition of NADG. The red curve elucidates the concentration of lectin whereas the blue curve indicates a decrease in fluorescence intensity of lectin on the reaction between 5×10^{-8} and 6×10^{-7} M of NADG. (b) Logarithmic plot of the lectin-NADG system at room temperature.

3.2. Encapsulation of drug content and drug loading

In the next step, the drug encapsulation and loading capacity were calculated for the final nano-bioconjugate (NADG-Q-NLBCs) in the system and compared to the lone NLBCs consecutively. The drug content encapsulated within Q-NLBCs and NADG-Q-NLBCs was evaluated using HPLC and was found to be 81 ± 1.72 % and 69 ± 2.60 %, respectively. The details of the detected contents for the triplicate analysis for Q-NLBCs and NADG-Q-NLBCs have been represented in **Table 2.1**. In addition, drug loading percent was found to be 19.23 ± 1.4% and 16.43 ± 2.6 % for Q-NLBCs and NADG-Q-NLBCs system, respectively. The greater efficacy of drug content encapsulated within NLBCs is most likely due to the entrapment/adsorption of the drug at the surface of poly-L-lysine. The efficacy of drug content encapsulation was decreased for NADG-Q-NLBCs, possibly due to the dissociation of some

functionalities in the acetate buffer. It has already been discussed that the drug content encapsulation efficiency is dependent on the composition of lipid and the binding energy **[29]**. In the work of Garg *et al*., 2016, drug content encapsulation of 87.8% (methotrexate-laden lipid nanocarriers) and 84.3% (fucose-conjugated methotrexate-laden lipid nanocarriers) was reported **[4]**. Although the encapsulation efficiency is higher in these cases for other systems, they may also suffer due to severe cytotoxicity, resulting in poor specificity *in vitro* testing. Hence, a system synchronizing all the aspects, including high drug encapsulation, low cytotoxicity, and targeted drug delivery, is of clinical interest **[30]**.

Table 2.1. Determination of amount of Q in the designed nano-bioconjugate using HPLC

Sample	Standard Q Concentration (µg/mL)	Detected concentration (µg/mL)	Unencapsulated Q concentration (µg/mL)	Encapsulated efficiency (%)
Q-NLBCs	500.0	411.0 405.0 398.0	89.00 95.00 102.0	81 ± 1.72
NADG-Q-NLBCs	500.0	351.0 345.0 336.0	149.0 155.0 164.0	69 ± 2.60

3.3. Morphological characterization of nano-bioconjugate

The morphological surface of Q-NLBCs and NADG-Q-NLBCs was studied using SEM characterization, as shown in **Fig. 2.4.** In both cases, overall spherical structures were observed, indicating the successful solid lipid carrier formulation using a single emulsion solvent evaporation technique. In the case of Q-NLBCs, the spherical structures were smooth and possessed a diameter in the range of 2.0 µm **(Fig. 2.4a).** Upon addition of NADG onto Q-NLBCs, the size became relatively larger **(Fig. 2.4b)**. This was due to the attachment of NADG onto the surface of Q-NLBCs, which assisted in the surface roughness and size increment. This also indicates the successful conjugation of the NADG onto the Q-NLBCs to form NADG-Q-NLBCs nano-bioconjugate.

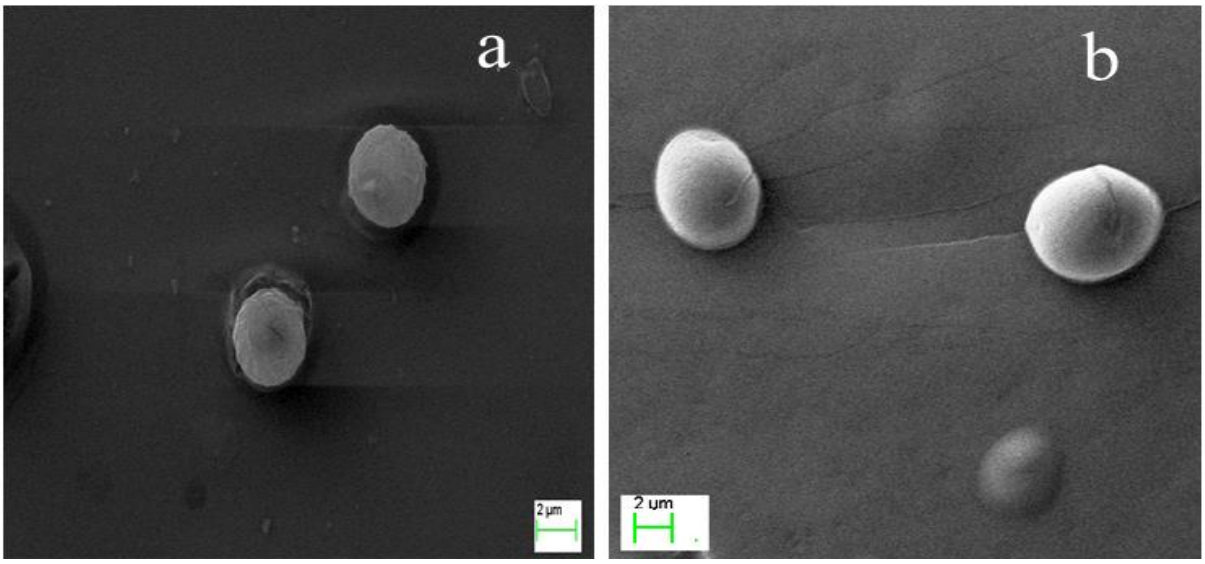

Figure 2.4. Scanning electron microscopy (SEM) photograph of the nano-bio material(a) Q-NLBCs and (b) NADG-Q-NLBCs

3.4. Average particle diameter and charge distribution measurement

The average diameter of Q-NLBCs and NADG-Q-NLBCs was measured using a nanoparticle analyzer. The particle size for Q-NLBCs was obtained to be 280 ± 3.12 nm (**Fig. 2.5a)**, while in the case of NADG-Q-NLBCs, it was found to be 390 ± 2.44 nm (**Fig. 2.5b)**. These results in terms of the larger size of NADG-Q-NLBCs than merely Q-NLBCs complement the results obtained using SEM. The average particle size of NADG-Q-NLBCs is greater than that of Q-NLBCs, suggesting the NADG has successfully coupled with NLBCs. Further, the sizes obtained through the zeta sizer vary with the sizes of particles obtained by SEM. One probable reason for such a change in size is that the SEM governs individual particle size, whereas the zeta sizer measures average particle size. Besides this, zeta sizer exposes the hydrodynamic diameter in an aqueous solution, whereas SEM measures the morphological size in the solid-state. The hydrodynamic diameter of the carrier is dependent on its concentration, henceforth, we diluted the suspension of the Q-NLBCs and NADG-Q-NLBCs samples to facilitate the

appropriate dispersion of the particles. Thus, the hydrodynamic diameter obtained using a zeta sizer is of nanometer range (nm) appropriate for diverse biological applications **[31]**.

Further, the surface charge for the final NADG-Q-NLBCs was calculated and compared to the system comprising only Q-NLBCs. The surface charge of a nano-bioconjugate system in the medium is a significant indicator of its stability. The zeta-potential value indicates the collective positive charges on the two nano bioconjugates surface. The overall surface charge was obtained to be 9.21 ± 0.74 mV and 11.22 ± 0.98 mV for NADG-Q-NLBCs and Q-NLBCs system, respectively. The absolute value of the positive charge is due to the amino group of poly-L-lysine, which is further reduced by adding NADG. Due to the overall positive charge of the carriers, their interactions with the cellular system may enhance and assist in the development of a potent lipid-based theranostic module.

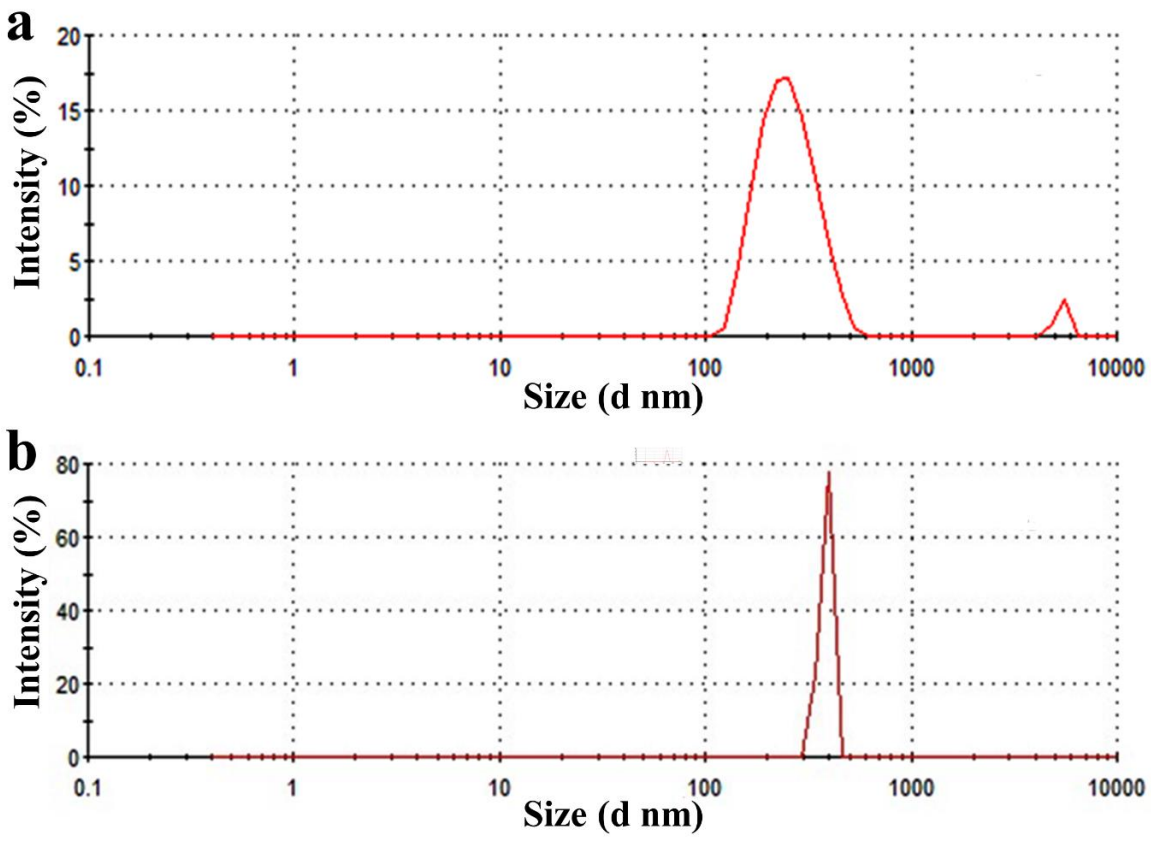

Figure 2.5. Distribution of hydrodynamic diameter in (nm) for (a) Q-NLBCs and (b) NADG-Q-NLBCs

3.5 IR characterization of nano-bioconjugate

The IR spectrum of Q-NLBCs (red curve) and NADG-Q-NLBCs (blue curve) (**Fig. 2.6**) was studied for the validation of numerous functionalities and their involvement in making bonds. The lipid spectrum shows the characteristic peak of the functionalities CH_2, OH, and PO_4^{3-} following the reported bands of lipid **[6,28,29,32]**. In the spectrum of Q-NLBCs, sharp peaks around 2915 cm^{-1}, 3390 cm^{-1}, 1629 cm^{-1} and 1047 cm^{-1} are observed, corresponding to CH2, OH, NH2, and PO_4^{3-}, respectively. These peaks obtained around the signature regions were due to the intrinsic functionalities of poly-L-lysine modified soya lecithin and Q in the tested system. Further, the spectrum of NADG-Q-NLBCs revealed that spectra keep intact the characteristic peaks due to CH_2, OH, NH_2, and PO_4^{3-} with the shifted band, however, the transmittance of the peak at 1629 cm^{-1} got reduced. Moreover, a new peak is observed in the spectra in the fingerprint region at 1425 cm^{-1}. This peak in the region is assigned to Schiff base or secondary amine, which is the result of the reaction involved between aldehyde groups of NADG and the surface-expressed amino groups of NLBCs. The ring-opening of NADG resulted in the free form of the aldehyde group that further interacts with amino expressed NLBCs. The shifting of the characteristics peaks to the higher wavenumber is a result of non-covalent interactions between NADG and lipids, such as electrostatic interaction, hydrogen bonding, Van der Waals forces, etc. These comparative analyses indicate the successful formation of NADG-Q-NLBCs nano-bioconjugate.

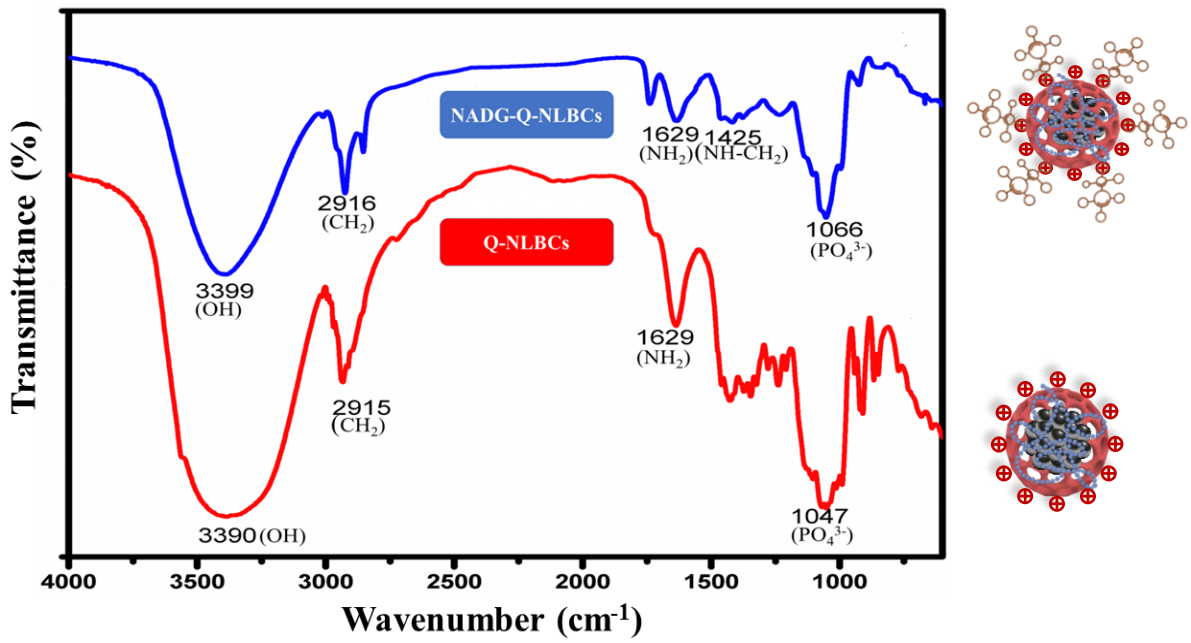

Figure 2.6. The infrared spectrum of Q-NLBCs and NADG-Q-NLBCs in the region of 4000–400 cm^{-1}.

3.6. X-ray characterization of nano-bioconjugate

X-ray diffraction studies were conducted for NLBCs and NADG-Q-NLBCs in separate experiments to characterize the nano-bioconjugate further. The X-ray scanning was made over 2θ, extending from 2° to 90°**.** The diffractogram showed a characteristic broad peak at 2θ = 23.9° which was merely due to the lipid in the composite **[33]** (**Fig. 2.7a)**. In this case, it was evident that the monomers used for NLBCs formulation were not in much-ordered form resulting in an amorphous structure; hence a broader peak has been observed. The distribution of diffraction peaks of the amorphous structure is due to the crystal's unstable states and the lack of absolute positive and destructive X-ray interference in a finite-sized lattice **[34]**. Interestingly, when we examined the NADG-Q-NLBCs systems, two sharp peaks are observed at 2θ = 26.5° and 2θ = 30.2° (**Fig. 2.7b**). The above results hypothesize that sharp peaks at the mentioned angles are due to the crystalline or ordered lipid bilayer. The crystallinity of the lipid layer is attained as a consequence of Q entrapment inside the core of the lipid carrier **[35].** The

aforementioned characterization clearly suggests the drug Q is successfully entrapped in the functionalized carrier that can be used for further application.

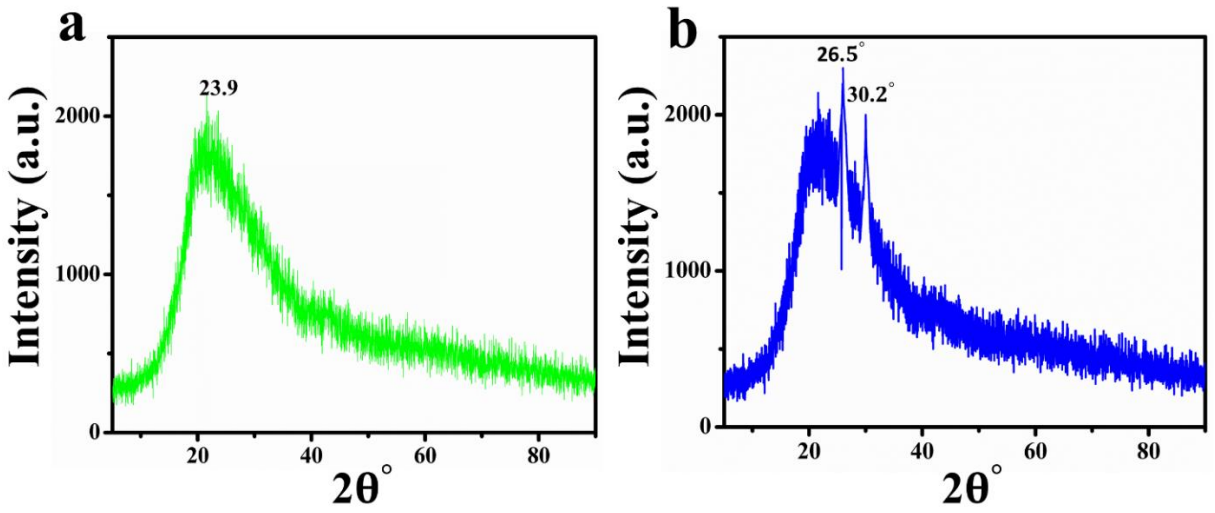

Figure 2.7. X-ray diffractogram of (a) NLBCs and (b) NADG-Q-NLBCs between 2θ = 2° to 2θ = 90° at a scanning speed of 0.03°/second.

3.7. Drug release kinetic

After characterizing the fabrication of the nano-bioconjugate and drug encapsulation, we further investigated the drug release in PBS buffer. The drug release pattern from fabricated nano-bioconjugate was studied for 200 h presented in **Fig. 2.8.** Zero-order and first-order kinetic models were used to determine whether the drug release behavior is concentration-dependent or independent **[36,37].** The zero-order pattern was obtained when data were plotted as cumulative percent drug release along Y-axis against time along X-axis (**Fig.2.8a**). To achieve the first-order pattern, data were plotted as log remaining percent of drug release along Y-axis against time along X-axis (**Fig. 2.8b**). The figures reveal that the drug release rate is faster initially, followed by a relatively slow drug release from the carrier. This kind of drug release behavior is obtained due to some drugs getting adsorb or making non-covalent interactions at the surface, and the remaining drugs reside in the subsequent layers of the NLBCs. During the process of lipids alignment to gain the solid structure, drugs are also

encapsulated in the core of lipid, which hampers drug release behavior. In order to achieve the constructive drugs release pattern, the linear regression analysis was applied in the zero and first-order plots as well. Based on effective drugs released from the nano-bioconjugates, the two regression lines are best fitted in the kinetic models separately. Further, the regression equations for the zero-order curve are expressed as: effective cumulative % of drug release up to 28.0 h (E) = 11.315 (± 3.951) + 1.072 (± 0.205) [Time], and effective cumulative % of drug release up to 200 h (E) = 39.825 (1.429) + 0.257 (± 0.010) [Time] with coefficient of determinants (R^2) of 0.945 and 0.988, respectively. Moreover, regression equations for the first order curve are expressed as: effective cumulative % of drug release up to 120 h (DRe) = 1.859 (± 0.025) + - 0.004(±0.001) [Time], and effective cumulative % of drug release up to 200 h (DRe) = 2.678 ± (0.094) + - 0.010 (± 0.001) [Time] with coefficient of determinants (R^2) of 0.932 and 0.972, respectively.

Figure 2.8. Drug release kinetics of Q from NADG-Q-NLBCs (*in vitro*) in phosphate buffer

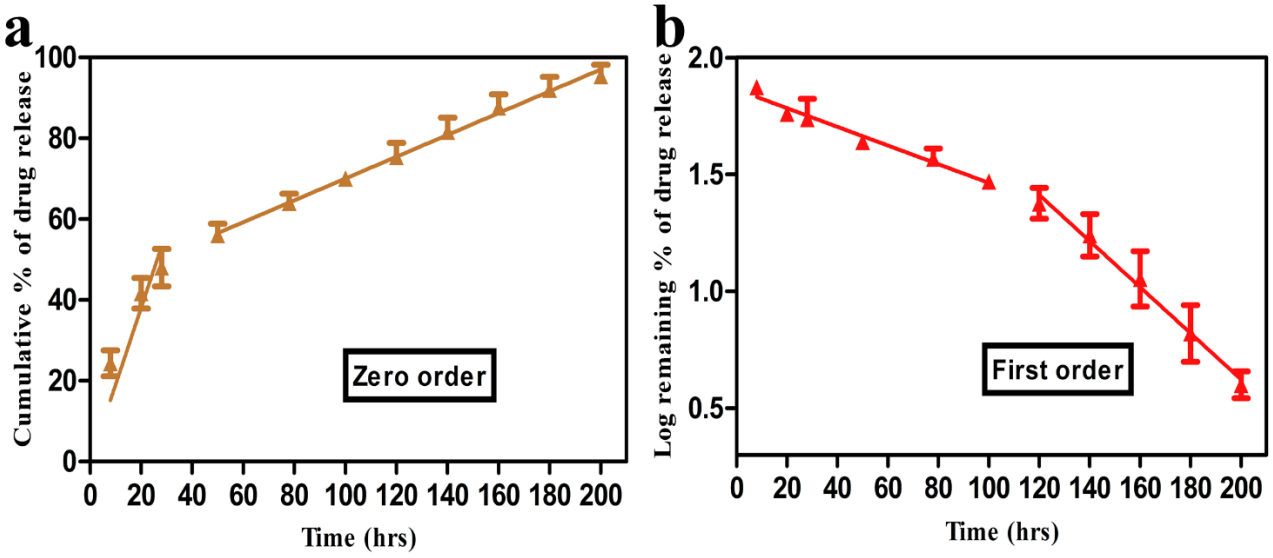

saline for (a) Zero-order and (b) First-order at physiological pH with a significance level ($p \leq 0.05^*$).

he relatively higher R^2 value signifies that the model is best fitted for the zero-order kinetic model, which means drug dissociation is a concentration-independent phenomenon. It can be

concluded from the above results that the multiple drug resistance can be controlled particularly in the diverse biological system with such type of nano-bioconjugate.

3.8. MTT assay

MTT assay was accomplished to estimate the cell cytotoxicity induced by NLBCs, free Q, and NADG-Q-NLBCs. In the experiment, MCF-7 cells were treated with five groups of inducers (NLBCs, free Q, and NADG-Q-NLBCs), and the first to the fifth group, the Q concentration was 2.0, 4.0, 6.0, 8.0, and 10.0 µg/mL. While in the formulation of NADG-Q-NLBCs, the Q concentration was similar to that of taking in the free form of Q (**Fig. 2.9**). The NLBCs without drug loading were taken as negative control (yellow bars), showing the maximum percent of cell viability. The viability of the cells was found to be 96 ± 1%, 97 ± 1%, 97 ± 2%, 98 ± 1% and 96 ± 1% for NLBCs at 2.0, 4.0, 6.0, 8.0, and 10.0 µg/mL, respectively. Further, cells induced with free Q at similar concentrations (blue bars), where the percentage of viable cells observed was 91 ± 1%, 85± 2%, 79 ± 2%, and 74 ± 2%, 69 ± 2%, respectively. In the final step, the NADG-Q-NLBCs nano-bioconjugate was tested under similar experimental conditions (green bars), where interestingly the % viability was lowest and found to be 78± 2%, 74 ± 1%, 65 ± 2%, 58± 2%, and 45 ± 3%, respectively. It is suggested from the data that the NLBCs are biocompatible and suitable for *in vitro* applications. However, NADG-Q-NLBCs showed significant cell toxicity at all the concentrations of Q, but the 'value of significance' is increased at a higher concentration (10.0 µg/mL) of Q in the system. The enhanced efficacy mechanism of cell toxicity of NADG-Q-NLBCs results from ligand NADG binds to the specific receptor lectin expressed on the cell surface of the MCF-7. The above results indicate that NADG-Q-NLBCs are the more effective carrier for accumulating Q inside the cells in a site-targeted manner. Further, we also evaluated the effect of inducers (NLBCs, free Q, and NADG-Q-NLBCs) on the non-cancer cells in the group at similar concentrations to assess their cell toxicity. The results suggest that the percent of cell viability was increased

for nanoformulation compared to free Q. In contrast, the percent of cell viability was found to be maximum for NLBCs formulation (figure not shown). In the comparison, the nano-bioconjugate does not accumulate the Q inside the non-cancer cells through receptor-mediated endocytosis. The lacking of the mechanisms mentioned above of cellular intake of the drugs may support the low expression of lectin receptors on the surface of the non-cancer cells **[38]**.

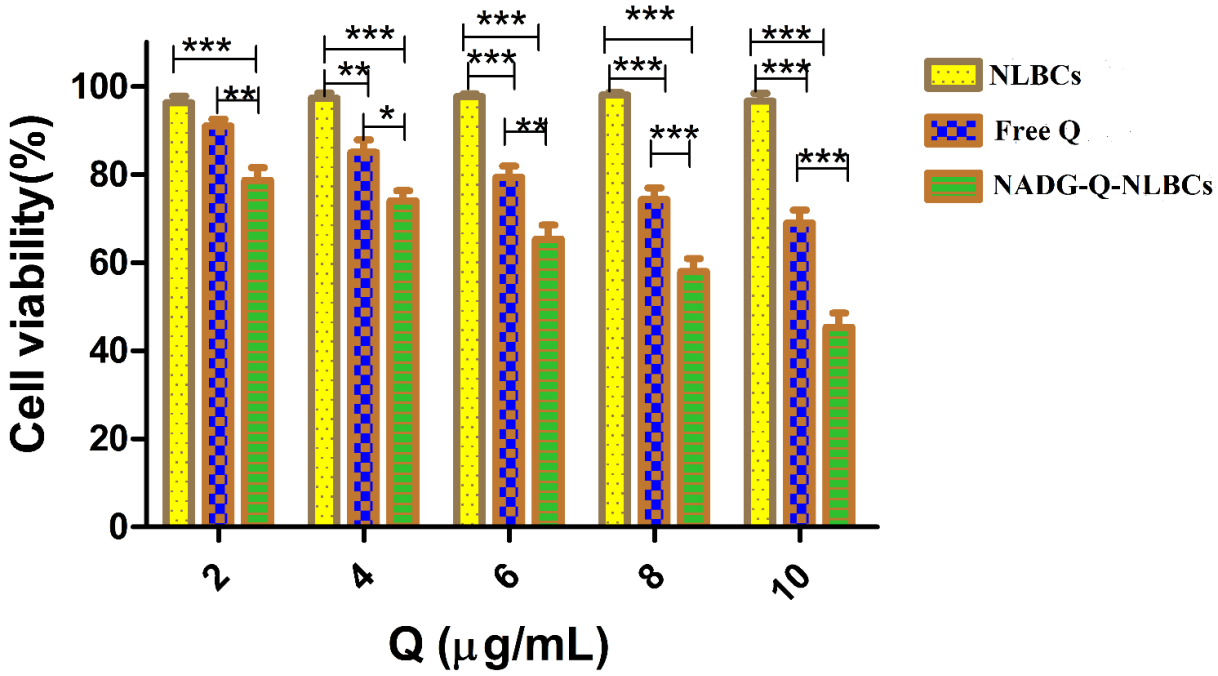

Figure 2.9. Cell toxicity studies on MCF-7 cells (*in vitro*). The histograms represent the % cell viability against NLBCs, free Q, and NADG-Q-NLBCs for five different concentrations at the cell's density of 4×10^5 cells/well. Values are reported as (mean ± standard error) and significance level as ($^{***}p< 0.001$, $^{**}p<0.01$ and $^{*}p<.05$). All experiments were performed in triplicates.

3.9. Analysis of cell apoptosis

It is known that apoptosis causes lipid irregularity, resulting in phosphatidylcholine and phosphatidylserine being exposed at the surface of apoptotic cells. Cells expressing phosphatidylserine at their surface are recognized and eliminated by the process of programmed cell death. Phosphatidylserine is an important component to maintain the symmetry and integrity of the cell membrane, and it has a high affinity for the dye annexin V

conjugated with FITC. Therefore, annexin V is used as a sensitive early apoptosis marker **[39]**. However, propidium iodide is permeable to the exposed membrane. It has a high affinity for nucleic acid, thus being employed as a marker for late apoptosis and necrosis of the cells. Hence, in our experiment, the MCF-7 cells were treated with NLBCs, Q-NLBCs, and NADG-Q-NLBCs, where the concentration of Q was kept constant (10.0 µg/mL). The treated cells were further characterized using a fluorescence-activated cell sorter with annexin V and PI (Double staining). Apoptosis of the cells induced by NLBCs, Q-NLBCs, and NADG-Q-NLBCs is displayed in **Fig. 2.10**. The quadrant Q3 represents viable cells (Annexin V^-, PI^-), Q4 and Q3 represent the early apoptotic cells (Annexin V^+, PI^-) and the late apoptotic cells (Annexin V^+, PI^+), respectively, and Q1 represents the necrotic cells (Annexin V^-, PI^+). It is observed that dot plots (Q3) show viable cells (**Fig. 2.10a),** whereas early and late apoptosis are noticed in the Q4 and Q2 quadrants, respectively (**Fig. 2.10b**). Furthermore, the percentage of early and late apoptotic cells increases in the Q4 and Q2 quadrants, respectively. (**Fig. 2.10c**). In cells, when treated with NADG-Q-NLBCs, the early apoptotic cells increased to 25.0 % at 10.0 µg/mL Q concentration in the NADG-Q-NLBCs formulation. The percentage of early apoptotic cells reached 10.0 % when treated with only Q-NLBCs at a similar concentration. The NADG-Q-NLBCs primarily induce apoptosis and necrosis of the cells. Apoptosis alters the cell at a morphological and biochemical level, whereas necrosis changes the cells at the physiological level **[40]**. Hence, the constructed NADG-Q-NLBCs nano-bioconjugate is the effective drug delivery vehicle that induces more apoptosis and supports the receptor-mediated endocytosis in the MCF-7 cells.

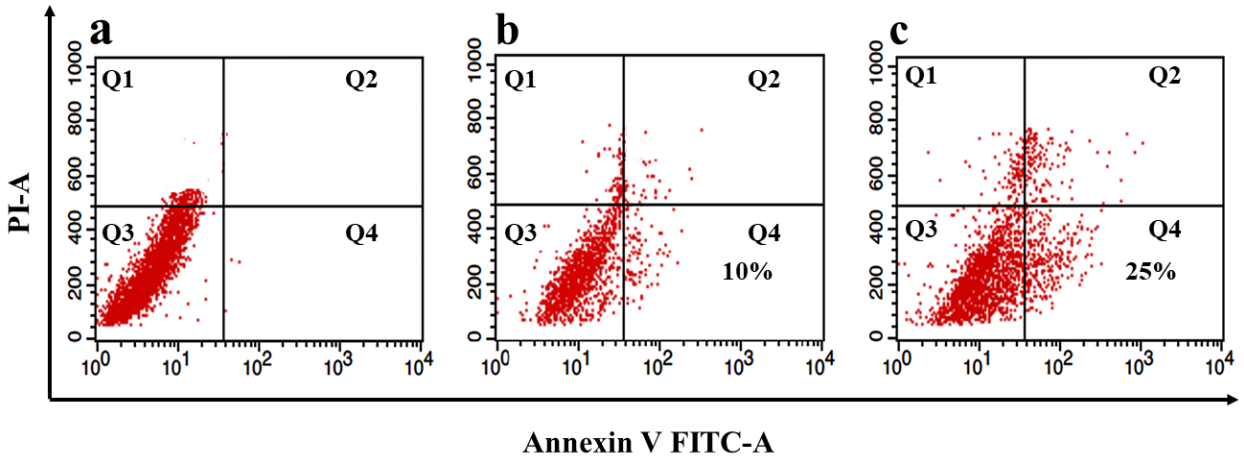

Figure 2.10. Flow cytometry images of MCF-7 cells (a) Cells treated with NLBCs for 48 h and dot quadrant Q3 showing the viable cells and Q1 represents the necrotic cells (b) Cells treated with Q-NLBCs for 48 h, quadrants Q4 and Q2 showing the early and late apoptotic cells, respectively and Q1 represents the necrotic cells (c) Cells treated with NADG-Q-NLBCs for 48 h, quadrants Q4 and Q2 indicating the early and late apoptotic cells, respectively and Q1 represents the necrotic cells. All experiments were performed in triplicates.

4. Conclusion

In this study, we have successfully designed NADG-Q-NLBCs nano-bioconjugate through the improved single emulsion solvent evaporation method. The charge interaction method carried the coupling of NADG to the surface of Q-NLBCs. Further, the constructed nano-bioconjugate was thoroughly characterized using SEM, particle size analyzer, IR spectroscopy, and XRD. The results obtained confirm the successful formation of NADG-Q-NLBCs which were, further applied for *in vitro* studies. The binding affinity between the lectin and NADG was confirmed using fluorescence spectroscopy. The release kinetics models were applied to verify the *in vitro* drug release behavior. These studies revealed that NADG-Q-NLBCs formulation is stable over time, initially releasing Q quickly and following a sustained pattern. Furthermore, the release kinetic graph shows that a total of 200 h is required for 100% drug release, which proves its efficacy for better sustain release. Moreover, the MTT assay confirmed that NADG-Q-NLBCs showed cytotoxicity at all the concentrations of Q. Through such nano-bioconjugate,

the maximum tolerated dose of drugs can be increased for effective therapy with the specificity towards breast cancer cells. In addition, the flow cytometry studies suggested the early and late apoptosis induced with NADG-Q-NLBC while cells induced with Q-NLBCs showed a less percentage of early apoptosis. However, the viability of cells reached the maximum for the cells treated with NLBCs. We conclude that the constructed nano-bioconjugate is capable of drug delivery at the targeted site and may also overcome multiple drug resistance which is a major impediment in cancer treatment. Future work can also be directed towards *in vivo* studies to collect sufficient data for systematic pre-clinical trial

5. References

[1] B. Yu, H.C. Tai, W. Xue, L.J. Lee, R.J. Lee, Receptor-targeted nanocarriers for therapeutic delivery to cancer, Molecular Membrane Biology. 27 (2010) 286–298. https://doi.org/10.3109/09687688.2010.521200.

[2] A. Yassemi, S. Kashanian, H. Zhaleh, Folic acid receptor-targeted solid lipid nanoparticles to enhance cytotoxicity of letrozole through induction of caspase-3 dependent-apoptosis for breast cancer treatment, Pharmaceutical Development and Technology. 25 (2020) 397–407. https://doi.org/10.1080/10837450.2019.1703739.

[3] K. Jain, P. Kesharwani, U. Gupta, N.K. Jain, A review of glycosylated carriers for drug delivery, Biomaterials. 33 (2012) 4166–4186. https://doi.org/10.1016/j.biomaterials.2012.02.033.

[4] N.K. Garg, B. Singh, A. Jain, P. Nirbhavane, R. Sharma, R.K. Tyagi, V. Kushwah, S. Jain, O.P. Katare, Fucose decorated solid-lipid nanocarriers mediate efficient delivery of methotrexate in breast cancer therapeutics, Colloids and Surfaces B: Biointerfaces. 146 (2016) 114–126. https://doi.org/10.1016/j.colsurfb.2016.05.051.

[5] A. Jain, P. Kesharwani, N.K. Garg, A. Jain, S.A. Jain, A.K. Jain, P. Nirbhavane, R. Ghanghoria, R.K. Tyagi, O.P. Katare, Galactose engineered solid lipid nanoparticles for targeted delivery of doxorubicin, Colloids and Surfaces B: Biointerfaces. 134 (2015) 47–58. https://doi.org/10.1016/j.colsurfb.2015.06.027.

[6] A. Jain, A. Agarwal, S. Majumder, N. Lariya, A. Khaya, H. Agrawal, S. Majumdar, G.P. Agrawal, Mannosylated solid lipid nanoparticles as vectors for site-specific delivery of an anti-cancer drug, Journal of Controlled Release. 148 (2010) 359–367. https://doi.org/10.1016/j.jconrel.2010.09.003.

[7] C. Bies, C.-M. Lehr, J.F. Woodley, Lectin-mediated drug targeting: history and applications, Advanced Drug Delivery Reviews. 56 (2004) 425–435. https://doi.org/10.1016/j.addr.2003.10.030.

[8] N.N. Palei, B.C. Mohanta, M.L. Sabapathi, M.K. Das, Lipid-based nanoparticles for cancer diagnosis and therapy, in: Organic Materials as Smart Nanocarriers for Drug Delivery, Elsevier, 2018: pp. 415–470. https://doi.org/10.1016/B978-0-12-813663-8.00010-5.

[9] H.-C. Siebert, N. van Nuland, U.M.S. Soedjanaatmadja, A. Rice, J.F.G. Vliegenthart, C.S. Wright, H.-J. Gabius, Role of aromatic amino acids in carbohydrate binding of plant lectins: Laser photo chemically induced dynamic nuclear polarization study of hevein domain-containing lectins, (n.d.) 17.

[10] S.M. Moghimi, A.C. Hunter, J.C. Murray, Nanomedicine: current status and future prospects, FASEB j. 19 (2005) 311–330. https://doi.org/10.1096/fj.04-2747rev.

[11] P.B. Storm, J.L. Moriarity, B. Tyler, P.C. Burger, H. Brem, J. Weingart, Polymer Delivery of Camptothecin against 9L Gliosarcoma: Release, Distribution, and Efficacy, (n.d.) 9.

[12] P. Kesharwani, V. Gajbhiye, N.K. Jain, A review of nanocarriers for the delivery of small interfering RNA, Biomaterials. 33 (2012) 7138–7150. https://doi.org/10.1016/j.biomaterials.2012.06.068.

[13] B. Petri, A. Bootz, A. Khalansky, T. Hekmatara, R. Müller, R. Uhl, J. Kreuter, S. Gelperina, Chemotherapy of brain tumour using doxorubicin bound to surfactant-coated poly(butyl cyanoacrylate) nanoparticles: Revisiting the role of surfactants, Journal of Controlled Release. 117 (2007) 51–58. https://doi.org/10.1016/j.jconrel.2006.10.015.

[14] P. Kesharwani, V. Mishra, N.K. Jain, Generation dependent hemolytic profile of folate engineered poly(propyleneimine) dendrimer, Journal of Drug Delivery Science and Technology. 28 (2015) 1–6. https://doi.org/10.1016/j.jddst.2015.04.006.

[15] A. Miglietta, R. Cavalli, C. Bocca, L. Gabriel, M. Rosa Gasco, Cellular uptake and cytotoxicity of solid lipid nanospheres (SLN) incorporating doxorubicin or paclitaxel, International Journal of Pharmaceutics. 210 (2000) 61–67. https://doi.org/10.1016/S0378-5173(00)00562-7.
[16] D. Volodkin, H. Mohwald, J.-C. Voegel, V. Ball, Coating of negatively charged liposomes by polylysine: Drug release study, Journal of Controlled Release. 117 (2007) 111–120. https://doi.org/10.1016/j.jconrel.2006.10.021.
[17] M. Michel, A. Izquierdo, G. Decher, J.-C. Voegel, P. Schaaf, V. Ball, Layer by Layer Self-Assembled Polyelectrolyte Multilayers with Embedded Phospholipid Vesicles Obtained by Spraying: Integrity of the Vesicles, Langmuir. 21 (2005) 7854–7859. https://doi.org/10.1021/la050497w.
[18] H. Takeuchi, H. Kojima, T. Toyoda, H. Yamamoto, T. Hino, Y. Kawashima, Prolonged circulation time of doxorubicin-loaded liposomes coated with a modi®ed polyvinyl alcohol after intravenous injection in rats, European Journal of Pharmaceutics and Biopharmaceutics. (1999) 7.
[19] L.A. Pham-Huy, H. He, C. Pham-Huy, Free Radicals, Antioxidants in Disease and Health, FREE RADICALS AND ANTIOXIDANTS. 4 (2008) 8.
[20] C. Saha, A. Kaushik, A. Das, S. Pal, D. Majumder, Anthracycline Drugs on Modified Surface of Quercetin-Loaded Polymer Nanoparticles: A Dual Drug Delivery Model for Cancer Treatment, PLoS ONE. 11 (2016) e0155710. https://doi.org/10.1371/journal.pone.0155710.
[21] M. Zhang, S.G. Swarts, L. Yin, C. Liu, Y. Tian, Y. Cao, M. Swarts, S. Yang, S.B. Zhang, K. Zhang, S. Ju, D.J. Olek, L. Schwartz, P.C. Keng, R. Howell, L. Zhang, P. Okunieff, Antioxidant Properties of Quercetin, in: J.C. LaManna, M.A. Puchowicz, K. Xu, D.K. Harrison, D.F. Bruley (Eds.), Oxygen Transport to Tissue XXXII, Springer US, Boston, MA, 2011: pp. 283–289. https://doi.org/10.1007/978-1-4419-7756-4_38.
[22] J. Hua, Z. Li, W. Xia, N. Yang, J. Gong, J. Zhang, C. Qiao, Preparation and properties of EDC/NHS mediated crosslinking poly (gamma-glutamic acid)/epsilon-polylysine hydrogels, Materials Science and Engineering: C. 61 (2016) 879–892. https://doi.org/10.1016/j.msec.2016.01.001.
[23] E.L. Vodovozova, E.V. Moiseeva, G.K. Grechko, G.P. Gayenko, N.E. Nifant'ev, N.V. Bovin, J.G. Molotkovsky, Antitumour activity of cytotoxic liposomes equipped with selectin ligand SiaLeX, in a mouse mammary adenocarcinoma model, European Journal of Cancer. 36 (2000) 942–949. https://doi.org/10.1016/S0959-8049(00)00029-0.
[24] P. Chandra, W.C.A. Koh, H.-B. Noh, Y.-B. Shim, In vitro monitoring of i-NOS concentrations with an immunosensor: The inhibitory effect of endocrine disruptors on i-NOS release, Biosensors and Bioelectronics. 32 (2012) 278–282. https://doi.org/10.1016/j.bios.2011.11.027.
[25] M. Choudhary, P. Yadav, A. Singh, S. Kaur, J. Ramirez-Vick, P. Chandra, K. Arora, S.P. Singh, CD 59 Targeted Ultrasensitive Electrochemical Immunosensor for Fast and Noninvasive Diagnosis of Oral Cancer, Electroanalysis. 28 (2016) 2565–2574. https://doi.org/10.1002/elan.201600238.
[26] M.H. Akhtar, K.K. Hussain, N.G. Gurudatt, P. Chandra, Y.-B. Shim, Ultrasensitive dual probe immunosensor for the monitoring of nicotine induced-brain derived neurotrophic factor released from cancer cells, Biosensors and Bioelectronics. 116 (2018) 108–115. https://doi.org/10.1016/j.bios.2018.05.049.
[27] S. Chung, P. Chandra, J.P. Koo, Y.-B. Shim, Development of a bifunctional nanobiosensor for screening and detection of chemokine ligand in colorectal cancer cell line, Biosensors and Bioelectronics. 100 (2018) 396–403. https://doi.org/10.1016/j.bios.2017.09.031.

[28] P. Chandra, S.A. Zaidi, H.-B. Noh, Y.-B. Shim, Separation and simultaneous detection of anticancer drugs in a microfluidic device with an amperometric biosensor, Biosensors and Bioelectronics. 28 (2011) 326–332. https://doi.org/10.1016/j.bios.2011.07.038.
[29] Y. Liu, J. Pan, S.-S. Feng, Nanoparticles of lipid monolayer shell and biodegradable polymer core for controlled release of paclitaxel: Effects of surfactants on particles size, characteristics and in vitro performance, International Journal of Pharmaceutics. 395 (2010) 243–250. https://doi.org/10.1016/j.ijpharm.2010.05.008.
[30] R. Kumar, D.K. Choudhary, M. Debnath, Development of BSA conjugated on modified surface of quercetin- loaded lipid nanocarriers for breast cancer treatment, Mater. Res. Express. 7 (2020) 015411. https://doi.org/10.1088/2053-1591/ab6774.
[31] A.K. Jain, S. Thareja, *In vitro* and *in vivo* characterization of pharmaceutical nanocarriers used for drug delivery, Artificial Cells, Nanomedicine, and Biotechnology. 47 (2019) 524–539. https://doi.org/10.1080/21691401.2018.1561457.
[32] M.M. Mady, W.M. Elshemey, Interaction of dipalmitoyl phosphatidylcholine (DPPC) liposomes and insulin, Molecular Physics. 109 (2011) 1593–1598. https://doi.org/10.1080/00268976.2011.575408.
[33] B. Nagaraj, C. Tirumalesh, S. Dinesh, D. Narendar, Zotepine loaded lipid nanoparticles for oral delivery: development, characterization, and in vivo pharmacokinetic studies, Futur J Pharm Sci. 6 (2020) 37. https://doi.org/10.1186/s43094-020-00051-z.
[34] B. Akbari, M.P. Tavandashti, M. Zandrahimi, Particle Size Characterization of Nanoparticles – a practical approach, 8 (2011) 9.
[35] M. Chu, Wu, A gold nanoshell with a silica inner shell synthesized using liposome templates for doxorubicin loading and near-infrared photothermal therapy, IJN. (2011) 807. https://doi.org/10.2147/IJN.S16701.
[36] Z.-L. Miao, Y.-J. Deng, H.-Y. Du, X.-B. Suo, X.-Y. Wang, X. Wang, L. Wang, L.-J. Cui, N. Duan, Preparation of a liposomal delivery system and its in vitro release of rapamycin, Experimental and Therapeutic Medicine. 9 (2015) 941–946. https://doi.org/10.3892/etm.2015.2201.
[37] M.M. Nounou, L.K. El-Khordagui, N.A. Khalafallah, S.A. Khalil, In vitro release of hydrophilic and hydrophobic drugs from liposomal dispersions and gels, Acta Pharm. (2006) 14.
[38] N.N. Palei, B.C. Mohanta, M.L. Sabapathi, M.K. Das, Lipid-based nanoparticles for cancer diagnosis and therapy, in: Organic Materials as Smart Nanocarriers for Drug Delivery, Elsevier, 2018: pp. 415–470. https://doi.org/10.1016/B978-0-12-813663-8.00010-5.
[39] G. Koopman, C. Reutelingsperger, G. Kuijten, R. Keehnen, S. Pals, M. van Oers, Annexin V for flow cytometric detection of phosphatidylserine expression on B cells undergoing apoptosis, Blood. 84 (1994) 1415–1420. https://doi.org/10.1182/blood.V84.5.1415.1415.
[40] R. Gerl, Apoptosis in the development and treatment of cancer, Carcinogenesis. 26 (2004) 263–270. https://doi.org/10.1093/carcin/bgh283.

Chapter III

Development of BSA conjugated on modified surface of quercetin- loaded lipid nanocarriers for breast cancer treatment

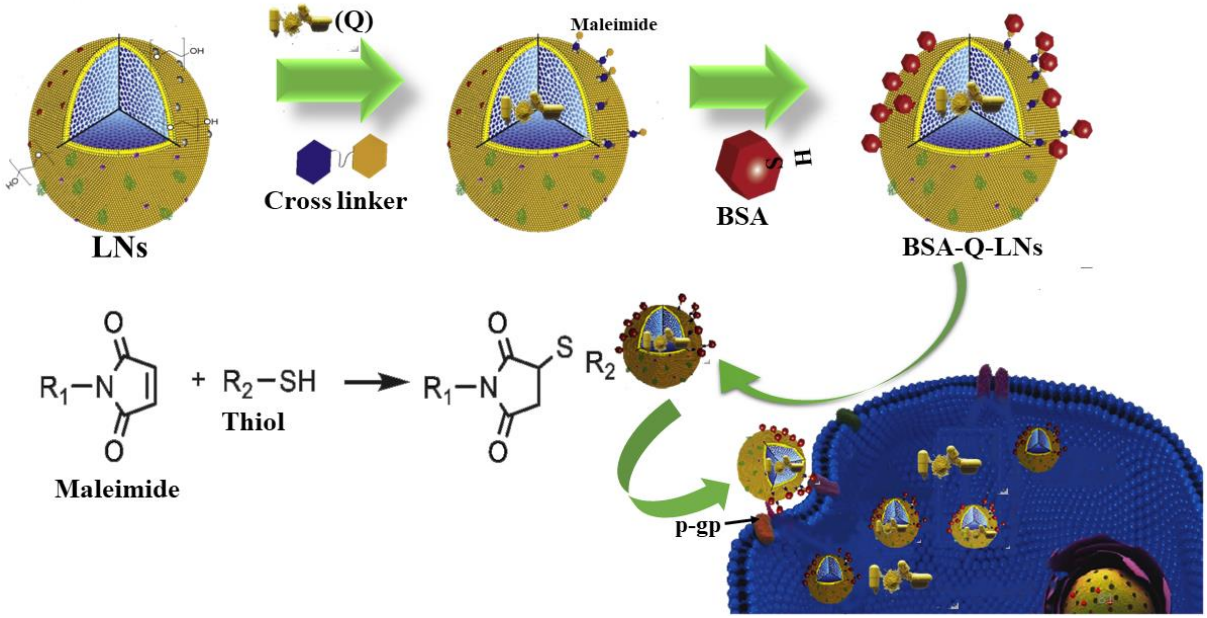

*Rahul Kumar et al., **Mater. Res. Express.** 7 (2020) 015411. doi.org/10.1088/2053-1591/ab6774*

Candidate CRediT and collaborators contribution statement

Rahul Kumar: Data curation, formal analysis, investigation, methodology, writing – thesis, review & editing, and conceptualization.

Collaborators: Review & editing, resource, validation, and software.

1. Introduction

The majority of anti-cancerous drugs have restrictions in clinical applications because of their poor solubility, and also show physiochemical and pharmaceutical behavior. The solubility of the drug can be improved by adding the adjuvant but when the drug is applied intravenously, the adjuvant may show adverse effects. These complications can be overcome using nanoformulation through biocompatible natural polymer **[1]**. In various studies, numerous biopolymers such as chitosan, gelatin, protein, polysaccharide, PLGA, and lipid are used for drug delivery application. Lipid nanocarriers (LNs) have the potential to solubilize, encapsulate, and deliver several bioactive drugs including anticancer drugs (quercetin, doxorubicin, and mitoxantrone) in a planned manner to achieve the accumulation of drugs inside the cancerous cells **[2]**. The LNs have advantages such as constant release of drug, and biodegradability at high efficiency **[3]**. In addition, lipid-based formulations containing cytotoxic agents, prevent passive diffusion of encapsulated drugs into healthy cells and as a result circulation time increases. Moreover, lipid nanocarrier have been formulated to reduce the toxic effect of drugs in different organs by varying its biodistribution and pharmacokinetics. However, LNs have quick opsonization when taken by the reticuloendothelial system **[4]**. This problem has been resolved by lipid grafted with maleimide. The modification of the lipid surface by the maleimide in the stepwise manner **[5]**, makes them stealth drug carrier (lipid) barren of long circulatory in nature & opsonization. The LNs are used as a matrix material for drug encapsulation and can be chosen from a variety of lipids, including phospholipids, cholesterol and triglycerides **[6]**. The amphiphilic nature of phospholipid allows to form organized structure, such as carriers when hydrated in aqueous environment **[7]**. The polymerization of phospholipid monomer is dependent on transition temperature, this is the temperature at which the lipids undergo fluidic conversion **[8]**.

The substantial progress towards the use of LNs in cancer therapy is the exploitation of the expressed receptors on the cancer cells through anchoring the receptor-mediated ligand to decorate the surface of LNs. Malignant cells generally overexpress receptor-like epidermal growth factor (EGFR), folate receptor (FR), estrogen receptor (ER), and P-glycoprotein receptor **[4]** showing greater affinity towards ligand. Thus, the efficacy of LNs can be improved more by targeting cancerous cells with the ligand anchored LNs followed by the receptor-mediated endocytosis of ligand decorated LNs. Further, various ligands (fucose, mannose, sialic acid, hyaluronic acid, and BSA) can be used for surface decoration to target the receptor expressed on cancerous cells **[9]**. The glycoprotein receptor expressed on the cancerous cell, specific for BSA. The targeting of BSA anchored liposome to the glycoprotein expressed cancerous cells may be an attractive approach.

In the background of drug delivery for the treatment of cancer, quercetin (Q) is most widely used anti-cancerous drugs. The chemical structure of Q counteracts the damage caused by free radicals in the living cells of our body. The cancerous cells are suppressed owing to the scavenging activity of the free radicals. In addition, Q is also known to have the capability to inverse the MDR pathway along with chemo preventive assets. Moreover, Q is also stated to impede the tyrosine kinase pathway, CYP 450 of enzyme cox protein resulting in the modulation of signal transduction and apoptosis **[10]**.

Our interest is to deliver the Q in a site targeted and controlled manner through the BSA conjugated surface-modified quercetin-loaded lipid nanocarriers. In the present investigation, the construction of a lipid-based nanocarriers for targeted drug delivery was made**.** In construction, Q was encapsulated inside the lipid core. Maleimide was functionalized on the surface of LNs through pegylated phospholipid. BSA was conjugated to anchored maleimide through thiol-maleimide bond **[11]**. The BSA conjugated Q-loaded LNs (BSA-Q-LNs) may capable of targeted delivery of Q to P-glycoprotein expressed cancerous cells. The

in vitro cytotoxicity BSA-Q-LNs were investigated and compared with the Q- loaded LNs (Q-LNs) as well as free Q. **Fig. 3.1** shows the schematic representation of the BSA conjugated Q-loaded LNs fabrication process and its interaction with the cancer cell.

2. Materials and methods

L-α-phosphatidylcholine(soybean), quercetin, 4-dimethylamino pyridine (DMAP), dichloromethane (CH_2Cl_2), BSA and pyridine were purchased from Sigma-Aldrich. Dipalmitoyl phosphatidylethanolamine-polyethylene glycol 2000 (DPPE-PEG_{2000}) was purchased from Nanocs Inc. Chloroform used was of analytical grade from Sun Traders. Phosphate buffer from Sigma- Aldrich was used. Human breast cancer cell line MCF-7 was taken from NCCS Pune and Eagle^s minimum essential medium (MEM), fetal calf serum (FCS 10), streptomycin (1mg/ ml), penicillin (100UI/ml) trypsin and EDTA solutions were taken from Merck. 3-(4,5-dimethylthiazol-2-yl)-2,5diphenyltetrazolium bromide (MTT) dye test (TLC purity p97.5%), dimethyl sulfoxide (DMSO) were purchased from Sigma – Aldrich. All reagents and solvents used in this work (unless specified) are either of HPLC grade or analytical grade.

2.1. Preparation of Q-loaded LNs

The Q-LNs were prepared using a single emulsion solvent evaporation technique. Phosphatidylcholine and pegylated phospholipid (DPPE-PEG2000) were taken in a ratio of 4:1 (wt./wt). This mixture was liquified with Q (1.0 mg/2.0 ml) in chloroform. Subsequently, this solution slowly hydrated with a 5% aqueous solution (8.0 ml) containing 0.9% saline, 5% dextrose, 10% sucrose, and distilled water, using a syringe at above the transition temperature. This emulsion was stirred for four hours at 25°C on a magnetic stir plate for evaporation of the organic solvent. The resulting solution was sonicated using a probe sonicator (model no. UP/200S; power input 50 watt) over an ice bath for (3 min; 30% amplitude). The formed Q-

LNs were recovered by ultracentrifugation at (10000 rpm, 7828g) for 20 mins at 4°C. The purified Q-LNs were washed using milli-Q water to remove unbound excess aqueous solution and free Q. The formed Q-LNs were frozen by slow freezing. The formed Q-LNs solution was stored inside a freezer at -20°C and subsequently, the nanocarriers were freeze-dried using lyophilizer (Labconco, catalog no. 7740060) at pressure (0.020 millibar) for 2 days to get the powdered form of Q-LNs.

2.2. Surface modification of Q-LNs with maleimide

The formed Q-LNs containing polyethylene glycol (1.0 g) were liquified in 10.0 ml of CH_2Cl_2 **[12]**. DMAP (6.0 mg) and pyridine (0.2 ml) were added with 132.0 mg of acid chloride (3-chloro-2,5-dioxo-1 pyrrolidinepropanoyl chloride, was previously prepared using the method reported by **[5]** at ambient temperature. Then, the reaction mixture was stirred for 4 hours and dichloromethane was evaporated and takes a solid form. Further, this solid was suspended in methanol and stirred for another one hour followed by centrifugation (10000 rpm, 7828g) and supernatant was decanted. Triethylamine was added into the resulting mixture and stirred for 4.0 hours for removal of the solvent. Finally, maleimide functionalized with Q-LNs were purified using ultracentrifugation.

2.3. Preparation of BSA conjugated with modified Q-LNs

Maleimide functionalized Q-LNs were conjugated with BSA through thiol reaction in which C_1 carbon of maleimide makes abound with the thiol group of BSA **(Fig. 3.2)**. All reaction mixture was evaporated under vacuum at 25°C using a rotary evaporator to remove any residual. The resulting solution was degassed by bubbling nitrogen for approximately 30 minutes. Standard solution of BSA (1.0 mg/ml) in degassed 0.1M NaCl (pH 6.2-6.5) was prepared formerly. Modified Q-LNs (5.0 ml) were incubated overnight at 37°C with a suitable volume of BSA stock solution under constant agitation in a shaker, at 180 rpm. The formed

BSA-Q-LNs were recovered by centrifugation at 10000 rpm, 7828g for 20.0 mins at 4°C and washed using milli-Q water to remove unbound BSA. Resulting formulations were freeze-dried through lyophilizer at pressure 0.020 millibar.

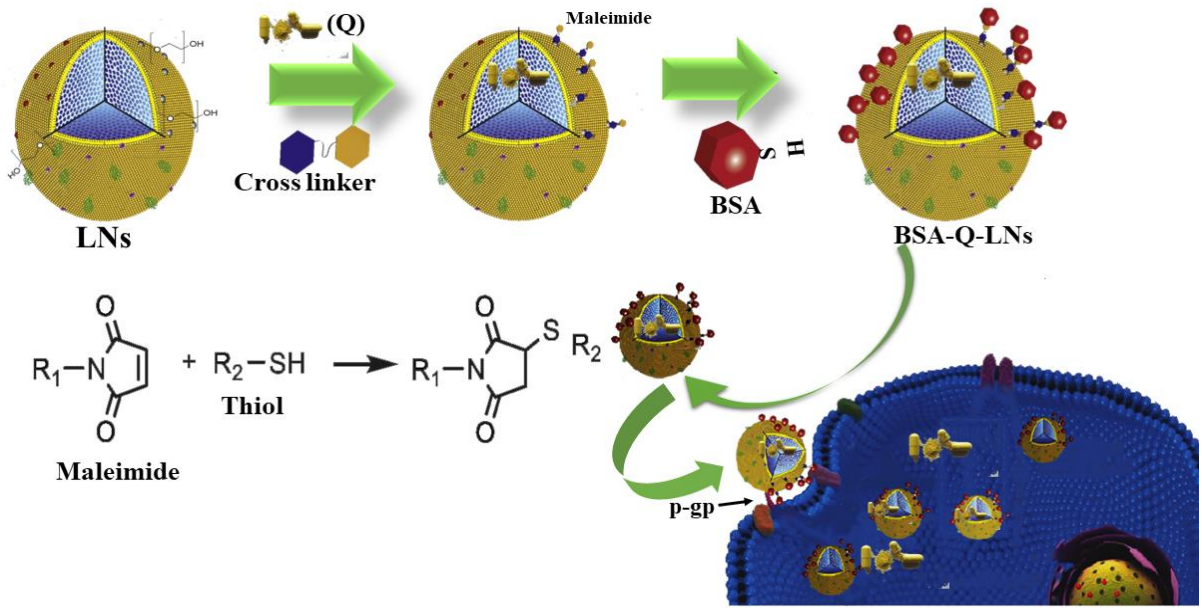

Figure 3.1. Schematic representation of the synthesis of BSA conjugated Q loaded lipid nanocarriers (LNs) and its cellular internalization through receptor mediated endocytosis.

2.4. Scanning electron microscope (SEM) studies

The surface features of void LNs, Q-LNs and BSA-Q-LNs were carried out by SEM ((Evo-Scanning Electron microscope MA15/18) operation at an accelerating voltage of 20.00 kV. A few drops of void LNs, Q-LNs, and BSA- Q-LNs suspensions were dried separately on a small rectangular glass cover, then coated with gold to make them conductive and placed on a copper stub prior to achievement of SEM image.

2.5. Particle size, size distribution, the surface charge of nano-bioconjugate

Nanoparticle analyzer (Malvern Paralytical Zetasizer Nano 486) was used to measure the size of the particles. The nano ZS incorporates non-invasive backscatter (NIBS^{TM}) optic that was used for size measurement. For the turbid sample, the detection angle was 173° which enabled

the size measurement. To determine the particle size, a dilute suspension of void, Q-loaded, and BSA anchored Q-loaded LNs (200.0µg/ml) was set in milli-Q water. Each was sonicated on an ice bath for one minute and then subjected to measurement of hydrodynamic diameter (nm). All the experiments were performed in triplicate. The value of the polydispersity index (PDI) was calculated using the equation 1:

$$PDI = \frac{M_w}{M_n} \qquad \ldots\ldots\ldots Eq.\ 1$$

where, M_w *and* M_n *denote weight-average molar mass and number average molar mass, respectively.*

2.6. Drug encapsulation efficiency

The encapsulation efficiency EE (%) was determined using UV-spectrophotometer (Fry et al). The Q-LNs (5.0 mg) were soaked with phosphate buffer saline(pH.7.4) for 30.0 mins. The whole solution was centrifuged at 10000 rpm, 7828g for 10 mins to separate unentrapped Q. The entrapped Q was determined by disrupting the lipid matrix with TritonX-100. The amount of Q collected were measured using UV-spectrophotometer. The EE (%) was calculated by the following equation:

$$\mathrm{EE}(\%) = \frac{\mathrm{Drug_{total}} - \mathrm{Drug_{free}}}{\mathrm{Drug_{total}}} \times 100 \qquad \ldots\ldots\ldots Eq.\ 2$$

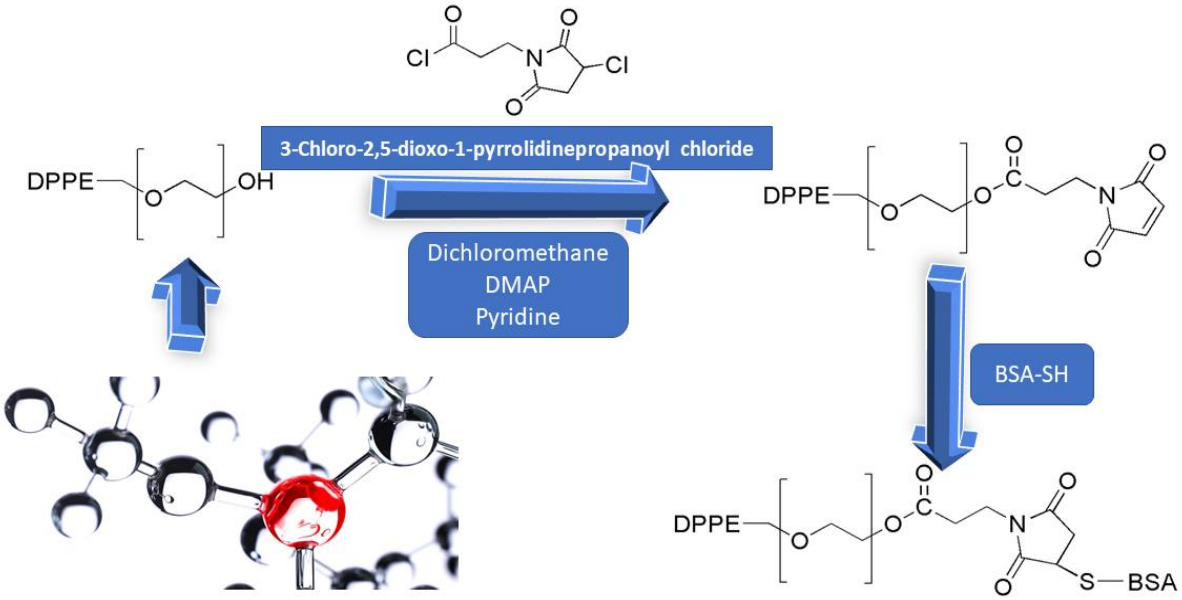

Figure 3.2. Chemical reactions for maleimide functionalization and BSA conjugation

2.7. Fourier transformed infrared spectroscopy (FT-IR)

FT-IR analysis was performed using model, Nicolet iS5. This analysis was conducted to verify the presence of various functional groups in lipid, Q, and BSA. During the experiment, the dried solid samples (1% by weight) were crushed to mix with potassium bromide and then pressed to make a pellet. Spectra were recorded for each sample at a spectral range between 4000 and 400 cm^{-1}.

2.8. XRD (X-ray diffraction study)

X-ray diffraction analysis **[13]** was performed to observe the crystalline structure of void, and BSA-Q loaded LNs using a (MiniFlex2 goniometer, Rigaku, Tokyo) with Cu Kα radiation, operating at 30kV/ 15mA. All the parameters were made at room temperature within the 2-theta range of 2° -80° at a speed of 1° min^{-1}.

2.9. In vitro release kinetics study

The dissociation of Q from LNs was performed by dissolving 4.0 mg of lyophilized Q loaded LNs in 2.0 ml of phosphate buffer saline solution (pH.7.4) which contains 0.1% v/v NaN3 to maintain a sink condition. The Q-LN suspension was equally divided into three tubes, each tube had 2.0 ml of solution because the experiment was performed in triplicate. This suspension was kept in the incubator shaker at 37°C, 150 rpm for 200.0 hrs. The suspension was taken at regular interval from these tubes and centrifuged at 10000 rpm, 7828g, 4°C for 10.0 mins. Pellet was taken, 2.0 ml of fresh PBS/NaN3 solution was added to each test tube for next interpretations. The obtained supernatant was lyophilized at pressure 0.02 millibar and dissolved in 2.0 ml of DMSO. The solution was centrifuged at 10000 rpm, 7828g for10 mins to collect the drug in the supernatant. The amount of Q collected was measured using UV-spectrophotometer.

2.10. Cell culture

Breast cancer cell line (MCF-7) was obtained from NCCS, Pune, India. Cells were cultivated in DMEM media comprising 10% FBS, 2.0 mM glutamine, 1.0 mM sodium pyruvate, 100 U/ml penicillin, 100 µl/ml streptomycin and 50.0 µmolar 2-mercaptoethanol in CO_2 incubator with 5% CO_2 at a 37°C.

2.11. MTT assay

Cell viability of MCF-7 was evaluated using 3-(4,5-dimethylthiazol-2-yl)-2,5-diphenyltetrazolium bromide (MTT) assay **[14]**.The free Q, Q-loaded LNs, and BSA conjugated Q-LNs were liquefied in DMSO to get a concentration of 10.0 µg/ml. The stock solution was kept at -20°C. All suitable working concentration in cell culture medium were prepared immediately prior to use. Viability of all Q derivatives were assayed using monolayer

culture. MCF-7 cells (1×10^4 cells/well) were seeded in 96- well-tissue plates properly and cultured for 3 days. Then the cells were washed once in PBS. The washed cells were treated with free Q and using different concentrations of Q Viz.2.0, 4.0, 6.0, 8.0 and 10.0 µg/mL in Q-LN and BSA-Q-LN. They were incubated for 48.0 h. All the free Q, Q-LNs and BSA-Q-LNs were removed and 10µl of MTT solution (0.5 mg/ml) was added to each well. Finally, 150.0 µl DMSO (0.1-0.5%) was added to dissolve the formazan crystals. Absorbance was evaluated using spectrophotometer at 540 nm.

2.12. Confocal microscopy

The morphological analysis of MCF-7 induced with free Q, Q-loaded LNs, and BSA conjugated Q-LNs were assayed by using ZEISS LSM780 confocal microscopy. Cells were grown in 12 well plates at density 4×10^4 cells per well and cultured for 24 hours. The media was removed and fresh media containing Q, Q-LNs, and BSA-Q-LNs were added with Q concentration of 10.0 µg/ ml. The treated cells were incubated for 48.0 days. After that, the incubated cells were swept away with PBS solution thrice and then cells were immobilized with 4% paraformaldehyde for 10 minutes.

2.13. DAPI Staining

DAPI staining protocol was followed by the modified procedure **[15]**. Paraformaldehyde (3%) was applied for treated MCF-7 cells. Cells were permeabilized with 0.2% Triton X-100 in phosphate-buffered saline (PBS). 20 µl of 5 mg/ml of DAPI was added into each sample and air-dried. Samples were visualized by ZEISS LSM780 confocal microscope.

2.14. Propidium Iodide (PI) Staining

PI staining protocol was exploited for the evaluation of intracellular localization of Q inside the MCF-7 cells. It was permeabilized with a blend of acetone: methanol (1:1, vol/vol) at 37ºC

for 10 minutes. Then PI (10 µL) was added to each sample and fixation was done by air drying. It was detected beneath ZEISS LSM780 confocal microscopy.

3. Results and Discussion

3.1. SEM analysis

SEM images of the void LNs, Q-LNs and BSA-Q-LNs are shown in **Fig. 3.3,** which confirmed the successful formation of LNs by the single emulsion solvent evaporation method. **Fig. 3.3A** shows the spherical structure which poses the diameter in the range of 2.0 µm**.** Further, it is observed that the surface morphology of the Q-LNs significantly changed by Q loading **(Fig. 3.3B).** In this study, 76% of Q was loaded inside the LNs results in shifting of void LNs from smooth to rough surface. The SEM image of BSA conjugated Q-loaded LNs is represented in **Fig. 3.3C**. From the image, it is revealed that the morphology of the formulation changed, evidencing the successful conjugation of BSA with Q-LNs. The SEM image of BSA conjugated Q-loaded LNs is validated using reported image of surface-modified LNs **[16]** and **[17]**

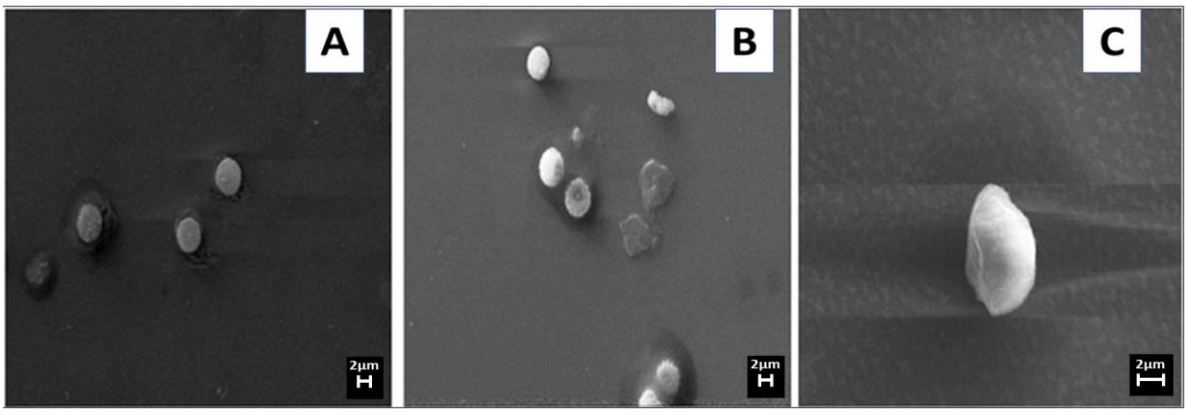

Figure 3.3. SEM image of (a) void LNs (b) Q-loaded LNs (c) BSA conjugated Q-LNs.

3.2. Size measurement analysis/Encapsulation efficiency

The particle size and size distribution of Q-LNs, BSA-Q-LNs were measured using a zeta sizer. The detail of particle size and size distribution of the formulations are illustrated in **Table 3.1**. The general sizes of the particles are obtained in the range of 200-300 nm with a polydispersity of 0.10 - 0.16, which is not a very broad size distribution. Moreover, BSA molecules affect the formulations' size and increase their diameter. The characterization mentioned above suggests that there may be effective conjugation between the thiol group of the BSA with C1 carbon of maleimide. This was also chemically confirmed using FTIR analysis, discussed in section 3.3. Further, the size obtained through the zeta sizer differs from the size when evaluated using SEM. The above outcome is demonstrated in the fact of SEM governs the morphological size in a solid-state while the zeta sizer exposes the hydrodynamic diameter in the aqueous phase **[18]**. The particle size distribution index (PDI) is an important parameter that provides information on particle size distribution. A PDI of less than 0.2 implies that the particle size distribution is uniform. The Zeta potential of a nano-bioconjugate system in the medium is a significant indicator of stability, biological activity, and cellular interactions. The overall high value of zeta potential, either positive or negative, facilitates the strong repulsive forces among the carriers, preventing the agglomeration of the particles **[19]**. The negative charge on the Q-LNs and positive charge on BSA-Q-LNs system are indicated by the zeta-potential illustrated in **Table 3.1**. The absolute value of the positive charge due to a BSA group of the final nano-bioconjugate is bigger than the negative charge from the phosphate group in the lipid system. Due to the overall higher positive charges of the carriers in an aqueous environment, the stability of the nano-bioconjugate is enhanced.

The encapsulated drug content within the constructed Q-LNs and BSA-Q-LNs is a critical parameter to explain their diverse biological applications. **Table 3.1** shows the amount of drug encapsulated in Q-LNs and BSA-Q-LNs systems which were found to be 76 ± 0.5% and 80 ± 1 %, respectively.

Sample	Particle size (nm)	Polydispersity	Zeta potential (mV)	Encapsulated efficiency (%)
Q-LNs	236 ± 5.65	0.10 ± 0.038	-30 ± 0.91	80 ± 1%
BSA-Q-LNs	296 ± 4.90	0.16 ± 0.040	18 ± 2.5	76 ± 0.5%

Table 3.1. Shows the particle size distribution and encapsulation efficiency of Q-LNs and BSA-Q-LNs.

3.3. Fourier transformed infrared spectroscopy analysis

The FT-IR spectra of void LNs, Q-loaded LNs and BSA conjugated Q-LNs are illustrated in **Fig. 3.4** respectively. The spectra shows the characteristics peak of the functional group CH_2, OH, C = O, PO_4^{3-}, and CH bands in the agreement with the reported spectra of lipid **[20,21,22,23]**, Q **[24]** and BSA **[25,26]**. The CH_2 stretching and bending bands of extended acyl chain of the void LNs are observed at 2930 cm^{-1} and 1350 cm^{-1} respectively. The band around 3450 $cm^{-1}$and 3452cm^{-1} is assigned to OH stretch which is intrinsic of lipid, Q, and BSA. In the spectra, C = O peak is observed at 1700 cm^{-1}. The C = O widening vibration of the ester group of phospholipids is in usual near-infrared section to govern the structural phase of membrane lipids. The peak at 1090 cm^{-1} is due to the phosphate group. The spectra of Q-LNs also engaged the characteristic peak as observed in void LNs with a slight shifting of OH peak. Moreover, the spectra of BSA conjugated Q-LNs involved the characteristics peak with the shifted band. The new band at 1675 cm^{-1} in the spectra is allotted to the amine group from the BSA. Further in this spectrum the characteristic peaks are shifted to the left due to the

surface modification of the lipid with maleimide. In addition, reduction in the absorption of some characteristic lipid band may be attributed to the formation of weak forces such as hydrogen bond, van der waals attractive forces or dipole-dipole interaction between lipid surface and maleimide. These shifts in peeks are due to the aforementioned interactions, support the successful Q- loading and BSA conjugation.

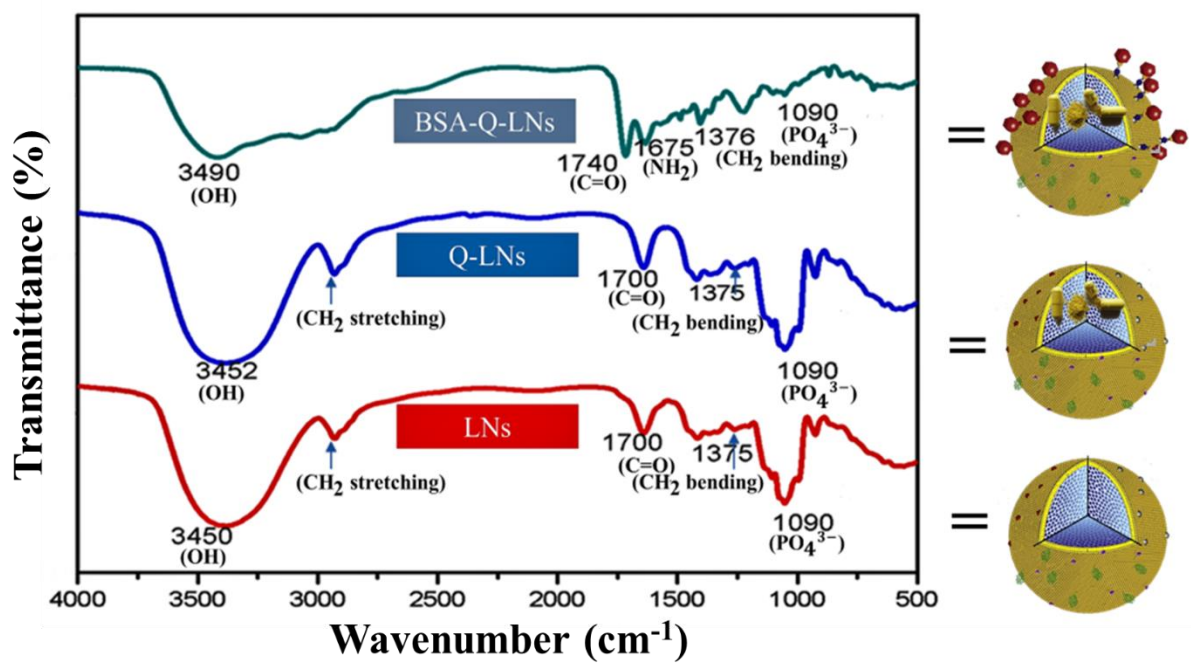

Figure 3.4. FT-IR spectra in the section of 4000–400 cm−1 (a) void LNs(b) Q-loaded LNs(c) BSA conjugated Q-LNs.

3.4. XRD analysis

XRD is used for characterization of void LNs and BSA-Q LNs for crystal structure analysis. From **Fig. 3.5**, the peak of XRD was recorded for void LNs and BSA-Q-LNs over 2-theta ranging from 2° to 80°. In the **Fig. 3.5a** no characteristic peak or broadened diffraction peak is observed for void LNs. This is attributed to amorphous nature or highly disordered crystal structure of LNs. The expansion of diffraction peaks is due to the chaotic states of crystal. This is attributed to the absence of total destructive and constructive interference of X-ray in a finite-sized lattice **[27]**.Also, the sharp characteristic peaks appeared at 2 theta =27.7° and 31.09°

in **Fig. 3.5b** exhibiting a polymorphic nature. This diffraction peak is due to the ordered or crystalline structure of the LNs. The ordered structure of the LNs is achieved due to the encapsulation of the Q inside the nanocarriers.

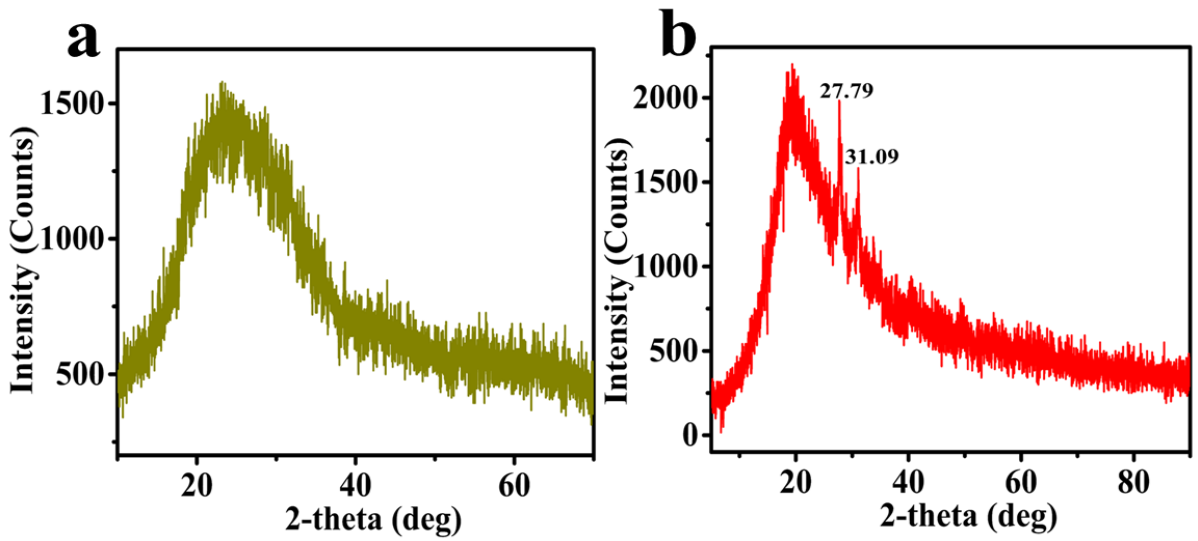

Figure 3.5. X-ray diffraction image of (a) void LNs and (b) BSA-Q-loaded LNs

3.5. Analysis of *in vitro* drug release kinetic

We performed the *in vitro* drug release kinetics for 200 h as presented in **Fig. 3.6**. It is observed that the drug release behavior is decreased after a successive period of time as some amount of drugs reside in the inner core and interact with lipids through weak bonds. The initial faster rate of release is commonly ascribed to drug detachment from the outer surface while later slow release is due to sustain drug release from the inner core of the LNs. In order to achieve the constructive drugs release pattern, the linear regression analysis was applied in the zero and first-order plots as well **[28**,**29]**. Based on effective drugs released from the nano-bioconjugates, the regression lines are best fitted in the kinetic models separately. Further, the regression equations for the zero-order curve are expressed as: effective cumulative % of drug release CDR = 28.85(± 2.46) + 0.331 (± 0.20) [Time], with coefficient of determinants (R^2) of 0.90. Moreover, regression equations for the first order curve are expressed as: effective cumulative % of drug release LDR = 1.904 (± 0.019) + - 0.004 (± 0.001) [Time] with

coefficient of determinants (R^2) of 0.95. The relatively higher R^2 value signifies that the model is best fitted for the first-order kinetic model, which means drug dissociation is a concentration-dependent phenomenon. This type of drug delivery system may overcome multiple drug resistance in biological system.

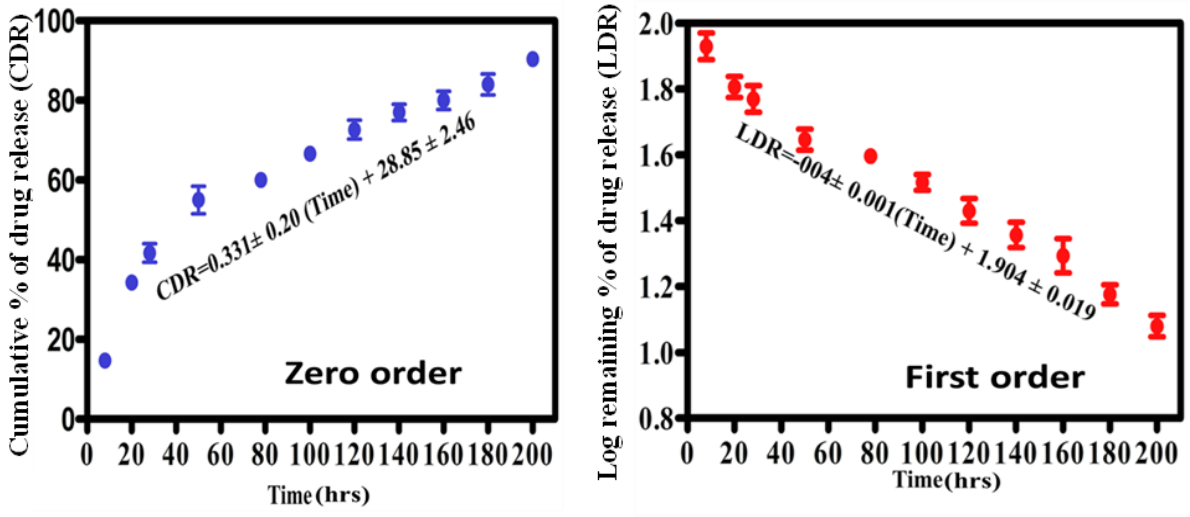

Figure 3.6. Release kinetic studies of BSA-Q-LNs (a) Zero-order release kinetics (b) First order release kinetic.

3.6. Cell Viability study

Cell viability study of free Q, Q-loaded LNs, and BSA conjugated Q-LNs are performed using MTT assay in monolayer culture for MCF-7 cells (**Fig. 3.7**). Briefly, MCF-7 cells were treated with five groups with inducers void LNs, Free Q, and, BSA-Q-LNs and the first to the fifth group; the Q concentration was 2.0, 4.0, 6.0, 8.0, and 10.0 µg/mL. While in the formulation of the BSA-Q-LNs, the MTX concentration was similar to that was taken in the free form of MTX. Void LNs without drug loading were taken as the control in the experiment, showing the maximum percent of cell viability. Further, cells induced with free MTX at similar concentrations, where the percentage of viable cells were observed to be 88.67 ± 1.87%, 85.67 ± 2.90%, 80.67 ± 2.09%, 76.00 ± 2.68%, and 70.00 ± 3.08%, respectively. For the cytotoxicity of BSA-Q-LNs formulation, similar concentrations of Q were applied and examined in dose

dependent manner. The percentage of viability was reduced to 80.09 ± 2.09%, 76.02 ± 4.79%, 69.02 ± 2.30%, 62.67 ± 3.49%, and 47.30 ± 2.11% after treatment with above formulation. Further, we also evaluated the effect of inducers on the non-cancerous cells in the group at similar concentrations to assess their cell toxicity. Results suggest that the percent of cell viability was significantly higher for the nano-formulations than Q (figure not shown). However, BSA-Q-LNs showed significant cell toxicity at all the concentrations of Q, but the 'value of significance' is increased at a higher concentration (10.0 µg/mL) of Q in the system. The enhanced efficacy mechanism of cell toxicity of BSA-Q-LNs results from ligand BSA may bind to the specific receptor P-gp expressed on the cell surface of the MCF-7 **[30]**. Further, a quantitative evaluation of the therapeutic potential of the dosages, the parameter $IC_{50,}$ is required. The following linear equation was used to calculate IC_{50}:

$$IC_{50} = (0.5 - b)/a \qquad \ldots\ldots\ldots\ldots Eq.\ 3$$

Where a and b denote slope and intercept, respectively.

The IC_{50} value was found to be 6.90 µg/mL for BSA-Q-LNs after 48.0 h of incubation

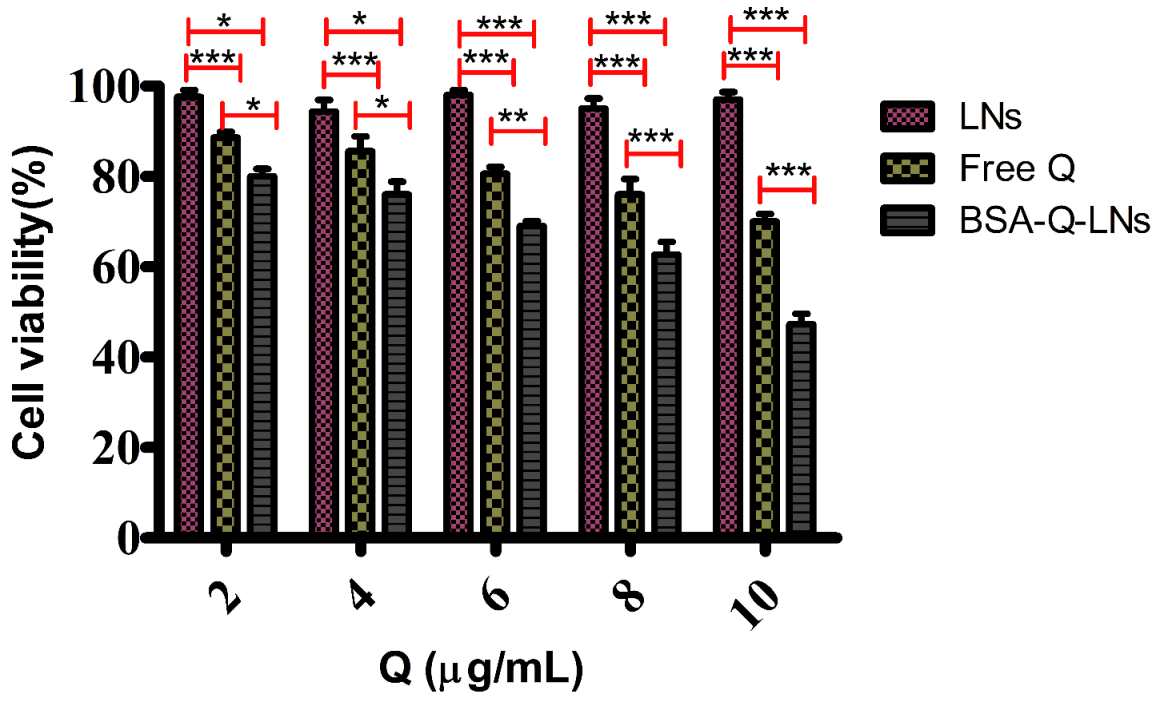

Figure 3.7. The cytotoxic effect of free Q, Q-loaded LNs, and BSA conjugated Q-LNs at various concentrations of Q on MCF-7.

3.7. Morphological analysis of MCF-7 induced with free Q, Q-LNs, and BSA-Q-LNs

The morphological changes induced with Q, Q-LNs, and BSA-Q-LNs system were assayed using confocal microscopy after 48.0 h of incubation. The fluorescence signals from the cells are illustrated in **Fig. 3.8**. The images obtained from DAPI staining display the blue fluorescence signals from the nucleus of the cells. However, the red fluorescence signals from propidium iodide staining also show the nucleus of the cells. Furthermore, cells treated with void LNs stabilized a large and clear nucleus after 48.0 h of incubation. The above findings suggest that the void LNs are biocompatible and suitable for biological applications. Further, compared to Q-LNs, BSA-Q-LNs induce more cell shrinkage with nuclear elongation and disintegration after mentioned incubation. The Q-LNs, and BSA-Q-LNs induced dose-dependent morphological changes in the nucleus of the cells, indicating more accumulation of the drugs. The cellular basis of internalization of BSA-Q-LNs is presumed to be cell fusion

followed by carrier-mediated endocytosis **[31]**. Henceforth it can be concluded BSA-Q-LNS is an excellent drug delivery vehicle in MCF-7 cells that enhances cellular toxicity of the drug as compared to Q-LNs.

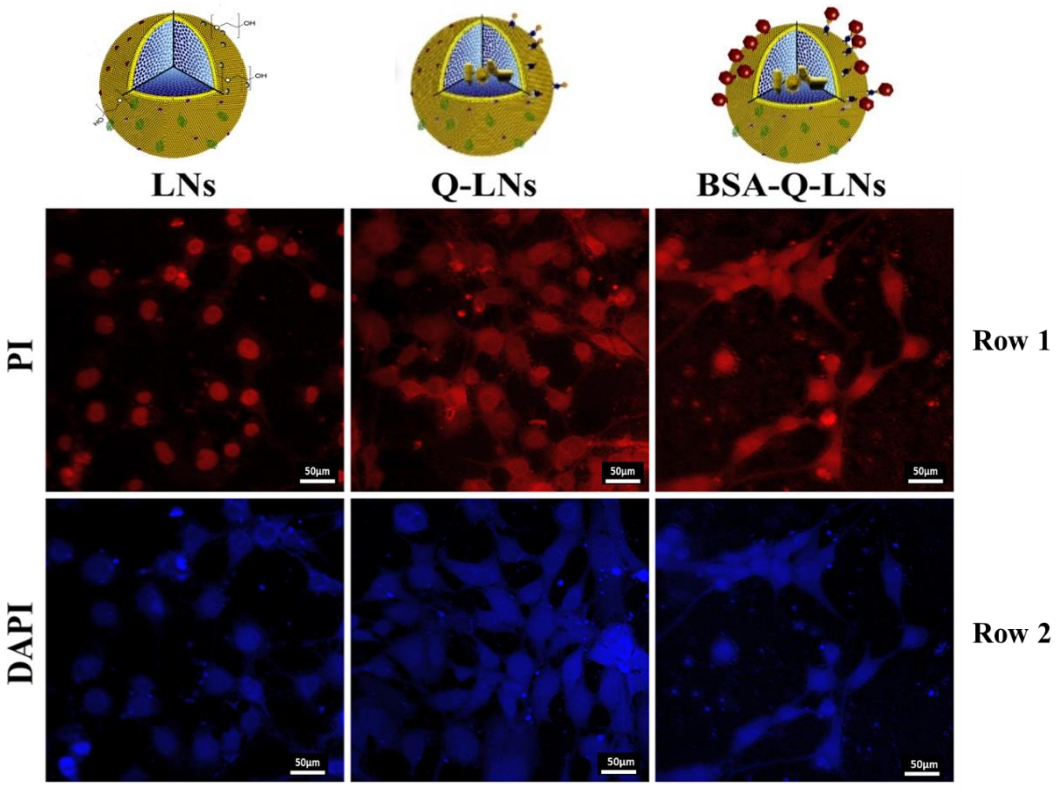

Figure 3.8. The confocal image of MCF-7, Row 1 cells treated with void LNs, Q-LNs, and BSA-Q-LNs; PI staining. Row 2 cells treated with void LNs, Q-LNs, and BSA-Q-LNs; DAPI staining.

4. Conclusion

In the present study, lipid nanocarrier is constructed which contains hydrophobic drugs (Q) in the core region and its surface is modified using maleimide. Further, BSA is conjugated with the modified surface of the lipid nanocarriers. This type of drug delivery system overcomes a certain limitation such as drug-like poor solubility, physiochemical and pharmaceutical behavior. This lipid-based nanocarrier is also capable of targeted drug delivery particularly in the case of cancerous cells. The SEM image confirmed the morphological differences that

occurred among void LNs, Q-LNs, and BSA-Q-LNs. The observed size of the formulated BSA-Q-LNs was found to be 296.43 ± 4.90 nm, which is suitable to enter the cell. Moreover, the FT-IR peak suggested the successful encapsulation of the Q and BSA conjugation with LNs. In addition, release kinetic was performed for 200 h, suggests the initial burst of Q followed by a constant release of Q from the core of the lipid matrix. Further, the constructed lipid-based nanocarriers are applied to analyze the cytotoxic effects in MCF-7 cells. It is observed that BSA conjugated Q-LNs accumulate more Q as compared to Q-LNs and free Q. The application of this Q-loaded nanocarriers on cancerous cell line K562 can also be investigated further and worth our consideration.

5. References

[1] T.M. Allen, C. Hansen, F. Martin, C. Redemann, A. Yau-Young, Liposomes containing synthetic lipid derivatives of poly(ethylene glycol) show prolonged circulation half-lives in vivo, Biochimica et Biophysica Acta (BBA) - Biomembranes. 1066 (1991) 29–36. https://doi.org/10.1016/0005-2736(91)90246-5.

[2] A. Yaghmur, O. Glatter, Characterization and potential applications of nanostructured aqueous dispersions, Advances in Colloid and Interface Science. 147–148 (2009) 333–342. https://doi.org/10.1016/j.cis.2008.07.007.

[3] T. Ramasamy, T.H. Tran, J.Y. Choi, H.J. Cho, J.H. Kim, C.S. Yong, H.-G. Choi, J.O. Kim, Layer-by-layer coated lipid–polymer hybrid nanoparticles designed for use in anticancer drug delivery, Carbohydrate Polymers. 102 (2014) 653–661. https://doi.org/10.1016/j.carbpol.2013.11.009.

[4] N.N. Palei, B.C. Mohanta, M.L. Sabapathi, M.K. Das, Lipid-based nanoparticles for cancer diagnosis and therapy, in: Organic Materials as Smart Nanocarriers for Drug Delivery, Elsevier, 2018: pp. 415–470. https://doi.org/10.1016/B978-0-12-813663-8.00010-5.

[5] S. Ji, Z. Zhu, T.R. Hoye, C.W. Macosko, Maleimide Functionalized Poly(ε -caprolactone)- *block* -poly(ethylene glycol) (PCL-PEG-MAL): Synthesis, Nanoparticle Formation, and Thiol Conjugation, Macromolecular Chemistry and Physics. 210 (2009) 823–831. https://doi.org/10.1002/macp.200900025.

[6] S.-Y. Chuang, C.-H. Lin, T.-H. Huang, J.-Y. Fang, Lipid-Based Nanoparticles as a Potential Delivery Approach in the Treatment of Rheumatoid Arthritis, Nanomaterials. 8 (2018) 42. https://doi.org/10.3390/nano8010042.

[7] Y. Zhu, M. Wang, J. Zhang, W. Peng, C.K. Firempong, W. Deng, Q. Wang, S. Wang, F. Shi, J. Yu, X. Xu, W. Zhang, Improved oral bioavailability of capsaicin via liposomal nanoformulation: preparation, in vitro drug release and pharmacokinetics in rats, Arch. Pharm. Res. 38 (2015) 512–521. https://doi.org/10.1007/s12272-014-0481-7.

[8] M.R. Mozafari, Nanoliposomes: Preparation and Analysis, in: V. Weissig (Ed.), Liposomes, Humana Press, Totowa, NJ, 2010: pp. 29–50. https://doi.org/10.1007/978-1-60327-360-2_2.

[9] A. Jain, A. Agarwal, S. Majumder, N. Lariya, A. Khaya, H. Agrawal, S. Majumdar, G.P. Agrawal, Mannosylated solid lipid nanoparticles as vectors for site-specific delivery of an anti-cancer drug, Journal of Controlled Release. 148 (2010) 359–367. https://doi.org/10.1016/j.jconrel.2010.09.003.

[10] J. Patten, S. Yang, IN RATS AND HUMAN LIVER MICROSOMES, (n.d.) 6.

[11] M.E. Gindy, S. Ji, T.R. Hoye, A.Z. Panagiotopoulos, R.K. Prud'homme, Preparation of Poly(ethylene glycol) Protected Nanoparticles with Variable Bioconjugate Ligand Density, Biomacromolecules. 9 (2008) 2705–2711. https://doi.org/10.1021/bm8002013.

[12] S.R. Paliwal, R. Paliwal, N. Mishra, A. Mehta, S.P. Vyas, A Novel Cancer Targeting Approach Based on Estrone Anchored Stealth Liposome for Site-Specific Breast Cancer Therapy, CCDT. 10 (2010) 343–353. https://doi.org/10.2174/156800910791190210.

[13] G.M. Shashidhar, B. Manohar, Nanocharacterization of liposomes for the encapsulation of water soluble compounds from *Cordyceps sinensis* CS1197 by a supercritical gas anti-solvent technique, RSC Adv. 8 (2018) 34634–34649. https://doi.org/10.1039/C8RA07601D.

[14] C. Di Meo, F. Cilurzo, M. Licciardi, C. Scialabba, R. Sabia, D. Paolino, D. Capitani, M. Fresta, G. Giammona, C. Villani, P. Matricardi, Polyaspartamide-Doxorubicin

Conjugate as Potential Prodrug for Anticancer Therapy, Pharm Res. 32 (2015) 1557–1569. https://doi.org/10.1007/s11095-014-1557-2.
[15] R. Rashmi, T.R. Santhosh Kumar, D. Karunagaran, Human colon cancer cells differ in their sensitivity to curcumin-induced apoptosis and heat shock protects them by inhibiting the release of apoptosis-inducing factor and caspases, FEBS Letters. 538 (2003) 19–24. https://doi.org/10.1016/S0014-5793(03)00099-1.
[16] H. Mishra, P.K. Mishra, Z. Iqbal, M. Jaggi, A. Madaan, K. Bhuyan, N. Gupta, N. Gupta, K. Vats, R. Verma, S. Talegaonkar, Co-Delivery of Eugenol and Dacarbazine by Hyaluronic Acid-Coated Liposomes for Targeted Inhibition of Survivin in Treatment of Resistant Metastatic Melanoma, Pharmaceutics. 11 (2019) 163. https://doi.org/10.3390/pharmaceutics11040163.
[17] S. Sana, S. Ghosh, N. Das, S. Sarkar, A.K. Mandal, Vesicular melatonin efficiently downregulates sodium fluoride-induced rat hepato- and broncho- TNF-α, TGF-β expressions, and associated oxidative injury: a comparative study of liposomal and nanoencapsulated forms, IJN. Volume 12 (2017) 4059–4071. https://doi.org/10.2147/IJN.S124119.
[18] N.K. Garg, B. Singh, A. Jain, P. Nirbhavane, R. Sharma, R.K. Tyagi, V. Kushwah, S. Jain, O.P. Katare, Fucose decorated solid-lipid nanocarriers mediate efficient delivery of methotrexate in breast cancer therapeutics, Colloids and Surfaces B: Biointerfaces. 146 (2016) 114–126. https://doi.org/10.1016/j.colsurfb.2016.05.051.
[19] H. Hu, D. Liu, X. Zhao, M. Qiao, D. Chen, Preparation, characterization, cellular uptake and evaluation *in vivo* of solid lipid nanoparticles loaded with cucurbitacin B, Drug Development and Industrial Pharmacy. 39 (2013) 770–779. https://doi.org/10.3109/03639045.2012.702348.
[20] M.M. Mady, W.M. Elshemey, Interaction of dipalmitoyl phosphatidylcholine (DPPC) liposomes and insulin, Molecular Physics. 109 (2011) 1593–1598. https://doi.org/10.1080/00268976.2011.575408.
[21] P. Alexander, M. Jainamboo, P.K. Praseetha, S.T. Gopukumar, SILICA COATED LIPOSOMES FOR DRUG DELIVERY TOWARDS BREAST CANCER CELLS, 9 (2016) 9.
[22] M.Y. Begum, M. Sudhakar, K. Abbulu, Flurbiprofen-Loaded Stealth Liposomes: Studies on the Development, Characterization, Pharmacokinetics, and Biodistribution, Journal of Young Pharmacists. 4 (2012) 209–219. https://doi.org/10.4103/0975-1483.104364.
[23] A. Blume, Properties of lipid vesicles: FT-IR spectroscopy and fluorescence probe studies, (n.d.) 14.
[24] A.M. Youssef Moustafa, A.I. Khodair, M.A. Saleh, Isolation, structural elucidation of flavonoid constituents from *Leptadenia pyrotechnica* and evaluation of their toxicity and antitumor activity, Pharmaceutical Biology. 47 (2009) 539–552. https://doi.org/10.1080/13880200902875065.
[25] P. Huang, Z. Li, H. Hu, D. Cui, Synthesis and Characterization of Bovine Serum Albumin-Conjugated Copper Sulfide Nanocomposites, Journal of Nanomaterials. 2010 (2010) 1–6. https://doi.org/10.1155/2010/641545.
[26] S. Servagent-Noinville, M. Revault, H. Quiquampoix, M.-H. Baron, Conformational Changes of Bovine Serum Albumin Induced by Adsorption on Different Clay Surfaces: FTIR Analysis, Journal of Colloid and Interface Science. 221 (2000) 273–283. https://doi.org/10.1006/jcis.1999.6576.
[27] B. Akbari, M.P. Tavandashti, M. Zandrahimi, PARTICLE SIZE CHARACTERIZATION OF NANOPARTICLES – A PRACTICALAPPROACH, 8 (2011) 9.

[28] Z.-L. Miao, Y.-J. Deng, H.-Y. Du, X.-B. Suo, X.-Y. Wang, X. Wang, L. Wang, L.-J. Cui, N. Duan, Preparation of a liposomal delivery system and its in vitro release of rapamycin, Experimental and Therapeutic Medicine. 9 (2015) 941–946. https://doi.org/10.3892/etm.2015.2201.
[29] M.M. Nounou, L.K. El-Khordagui, N.A. Khalafallah, S.A. Khalil, In vitro release of hydrophilic and hydrophobic drugs from liposomal dispersions and gels, Acta Pharm. (2006) 14.
[30] J. Wang, H. Ueno, T. Masuko, Y. Hashimoto, Binding of Serum Albumin on Tumor Cells and Characterization of the Albumin Binding Protein, The Journal of Biochemistry. 115 (1994) 898–903. https://doi.org/10.1093/oxfordjournals.jbchem.a124437.
[31] D. Manzanares, V. Ceña, Endocytosis: The Nanoparticle and Submicron Nanocompounds Gateway into the Cell, Pharmaceutics. 12 (2020) 371. https://doi.org/10.3390/pharmaceutics12040371.